Beam Energy Dependence of Triton Production and Yield Ratio ($N_t \times N_p/N_d^2$) in Au+Au Collisions at RHIC

(The STAR Collaboration)

We report the triton (t) production in Au+Au collisions at $\sqrt{s_{NN}}$ = 7.7 − 200 GeV measured at mid-rapidity ($|y| < 0.5$) by the STAR experiment from the first phase of the beam energy scan at the Relativistic Heavy Ion Collider (RHIC). The nuclear compound yield ratio ($N_t \times N_p/N_d^2$), which is predicted to be sensitive to the local density fluctuation of neutrons, monotonically decreases with increasing charged-particle multiplicity ($dN_{ch}/d\eta$) and exhibits a scaling behavior. The multiplicity dependence of the yield ratios are compared with calculations from coalescence and thermal models. Relative to the coalescence baseline, enhancements of the yield ratios are observed in the 0%-10% most central collisions at 19.6 and 27 GeV with a significance of 2.3σ and 3.4σ, respectively, with a combined significance of 4.1σ. The measured significance of these enhancements decreases with smaller p_T acceptance. The enhancements are not observed in peripheral collisions and model calculations without critical fluctuation. Important implications on the QCD phase structure and the production mechanism of light nuclei in heavy-ion collisions are discussed.

Quantum Chromodynamics (QCD) is the fundamental theory of the strong interaction. One of the main goals of the Relativistic Heavy Ion Collider (RHIC) is to explore the QCD phase structure [1, 2]. At high temperature and vanishing baryon chemical potential (μ_B = 0 MeV), Lattice QCD calculations demonstrate that the transition between hadronic matter and the Quark-Gluon Plasma (QGP) is a smooth crossover [3] and the transition temperature is about $T_c = 156$ MeV [4]. QCD-based model calculations suggest there is a first-order phase transition at large baryon chemical potential [5–8]. If theory postulations are correct, the first-order phase transition line should end at a critical point (CP) [9–11] toward the crossover region. A fundamental question is whether we can experimentally find the CP and pin down its location in the QCD phase diagram. The experimental confirmation of this landmark would be a milestone of exploring the QCD phase structure at finite baryon density [12–17].

Light nuclei, such as deuteron (d), triton (t), helium-3 (^{3}He), are loosely bound objects with binding energies of several MeV. Over the past half-century, the light nuclei production in heavy-ion collisions has been extensively studied both experimentally [18–28] and theoretically [29–43]. Two different mechanisms have been proposed to explain the generation of light nuclei at mid-rapidity, namely thermal production [44, 45] and nucleon coalescence [29, 32, 46]. Due to small binding energy, it is puzzling how light nuclei survive in the hot medium created in relativistic heavy-ion collisions implied by the success of the thermal model [47, 48]. By including hadronic effects in the Saha equation [36] or rate equation [49], model calculations demonstrate that the deuteron, triton and helium-3 yields remain unchanged during the hadronic expansion. A similar conclusion is obtained in a transport simulation of hadronic re-scattering processes realized by the dissociation and regeneration of deuterons via the reaction $\pi NN \leftrightarrow \pi d$ [35]. However, a recent calculation using the kinetic approach [50] demonstrates that the effects of hadronic re-scatterings during hadronic expansion also do not change the deuteron yield, but will reduce the triton and helium-3 yields by about a factor of 1.8 from their initial values given by thermal model. Therefore, systematic measurements of the triton and/or helium-3 yields over a broad energy range are important to clarify and understand the dynamics of light nuclei production in heavy-ion collisions.

In the coalescence production, light nuclei are not treated as point-like particles, but exhibit a finite size [29], and are formed via protons and neutrons that already passed kinetic freeze-out. When the radii of light nuclei are comparable to the size of the nucleon emission source in heavy-ion collisions, the yield of light nuclei will be significantly suppressed [29, 51, 52]. Recently, the compound yield ratio $N_t \times N_p/N_d^2$ of triton (N_t), deuteron (N_d), and proton (N_p), was predicted to be sensitive to the neutron density fluctuations in heavy-ion collisions. It is proposed as a sensitive observable to search for the signature of the CP and/or first-order phase transition [53–60], and is expected to show non-monotonic behavior as a function of collision energy. Due to the size effect in the coalescence production of light nuclei [51, 52], the yield ratio $N_t \times N_p/N_d^2$ monotonically increases with decreasing system size whereas a decrease with decreasing system size is predicted by the canonical thermal model [61]. Thus, this yield ratio can also serve as a powerful tool to distinguish different production mechanisms of light nuclei in heavy-ion collisions.

In this letter, we report triton production at mid-rapidity ($|y| < 0.5$) in Au+Au collisions at $\sqrt{s_{NN}}$ = 7.7, 11.5, 14.5, 19.6, 27, 39, 54.4, 62.4, and 200 GeV measured by the STAR experiment from the first phase of the Beam Energy Scan (BES-I, 2010-2017) program at RHIC [62]. The results presented are analyzed from minimum bias events of Au+Au collisions, occurring within +/-30 cm for 200 GeV and +/-40 cm for other energies of the nominal interaction point along the beam axis. Collision centralities are determined by fitting the measured charged particle multiplicities within pseudorapidity $|\eta| < 0.5$ with a Monte Carlo Glauber model [70]. The selected tracks are required to have a distance of closest approach (DCA) to the primary collision vertex of less than 1 cm and have at least 20 hit points measured in the Time Projection Chamber (TPC). The tritons are identified with the ionization energy loss, dE/dx, in the TPC [64] and with information from the Time-Of-Flight (TOF) detector [65]. To obtain the final triton p_T spectra, several corrections are applied on the raw p_T spectra. These corrections include the p_T dependent tracking efficiency, the low momentum energy loss correction, and the absorption correction due to the deficiency in the
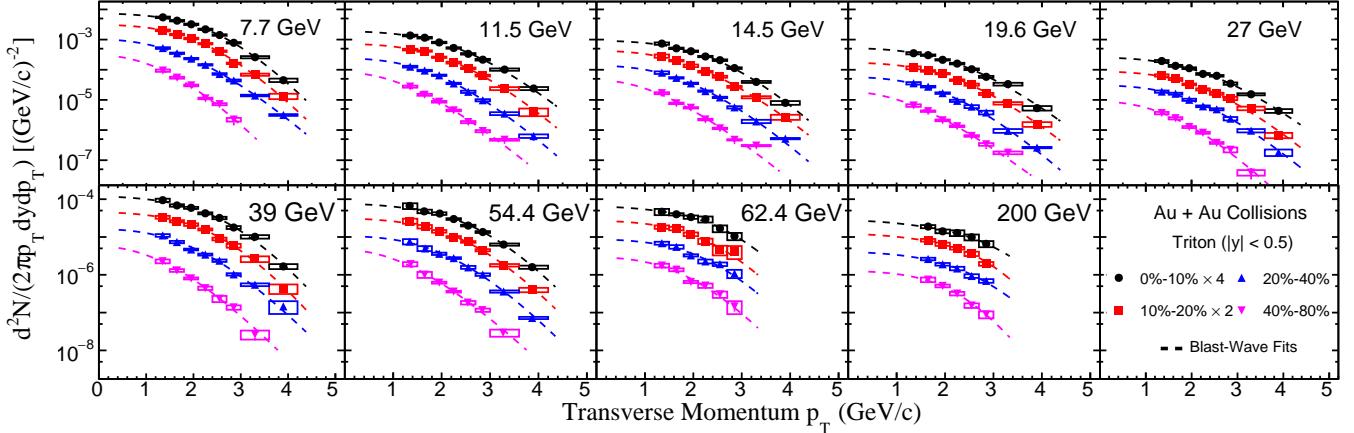
FIG. 1. Transverse momentum (p_T) spectra for mid-rapidity ($|y| < 0.5$) tritons from 0%-10%, 10%-20%, 20%-40%, and 40%-80% centralities in Au+Au collisions at $\sqrt{s_{NN}}$ = 7.7, 11.5, 14.5, 19.6, 27, 39, 54.4, 62.4, and 200 GeV. Dashed-lines are the corresponding Blast-Wave fits with the profile parameter n = 1. The statistical and systematic uncertainties are shown as vertical lines and boxes, respectively.

simulations, which were determined using embedding simulations [26, 66]. Because the TOF detector is used to identify tritons at high p_T, we also need to correct for the TOF matching efficiency, defined as the ratio of the number of tracks matched in the TOF to the number of total tracks in the TPC within the same acceptance. The point-to-point systematic uncertainties on the spectra are estimated by varying track selection, analysis cuts and by assessing the sample purity from the dE/dx measurement. Track selection and particle identification contribute by $\sim$3% and signal extraction contributes by less than $\sim$2% at low p_T and increasing to $\sim$10% at high p_T due to the reduced resolution of the TPC. A correlated systematic uncertainty of 5% is estimated for all spectra and is dominated by uncertainties in the Monte Carlo determination of reconstruction efficiencies. All of these uncertainties are added in quadrature to obtain the final systematic uncertainties.

Figure 5 shows the p_T spectra of identified tritons measured at mid-rapidity ($|y| < 0.5$) in Au+Au collisions at $\sqrt{s_{NN}}$ = 7.7, 11.5, 14.5, 19.6, 27, 39, 54.4, 62.4, and 200 GeV for 0%-10%, 10%-20%, 20%-40%, and 40%-80% centralities. The p_T-integrated particle yields (dN/dy) are calculated from the measured p_T range and extrapolated to the unmeasured regions with individual Blast-Wave model fits [67]. The extrapolation is an additional source of systematic uncertainty on dN/dy. This is estimated by comparing the extrapolation by different fit functions to the p_T spectra. The contribution to the yields from extrapolation is about 5%-20%, which is from the low p_T range. All of the mid-rapidity proton p_T spectra and dN/dy in Au+Au collisions at RHIC energies presented in this paper have been corrected for the weak decay feed-down via a data driven approach [68], which uses the inclusive proton spectra [69, 70] and the yields of strange hadrons measured by the STAR experiment [71] (See Supplemental note). In a previously published STAR paper [72], the proton feed-down correction was done by using a UrQMD + GEANT simulation, which underestimates the proton feed-down contributions from weak decays.

Figure 2 shows the energy dependence of dN/dy ratios, N_d/N_p [26] and N_t/N_p, in the mid-rapidity of central heavy-ion collisions from different experiments, including the FOPI [73], E864 [20], PHENIX [74, 75], and ALICE [27] experiments. Both the N_t/N_p and N_d/N_p ratios increase monotonically with decreasing collision energy and the differences between the ratios get smaller at lower collision energies. The solid lines represent the results calculated from the thermal model which does not include excited nuclei [76], in which the parametrization of chemical freeze-out temperature and μ_B from Ref. [77, 78] are used. Quantitatively, the thermal model describes the N_d/N_p ratios well, but it systematically overestimates the N_t/N_p ratios except for the results from central Pb+Pb collisions at $\sqrt{s_{NN}}$ = 2.76 TeV [27]. On the other hand, coalescence model can also describe energy dependence trends [52] and the production of light nuclei at mid-rapidity strongly depends on the baryon density ρ_B as $N_A/N_p \propto \rho_B^{A-1}$.

As mentioned earlier, the yield ratio $N_t \times N_p/N_d^2$ is predicted to be sensitive to the local baryon density fluctuations and can be used to probe the QCD phase structure. Figure 3 shows the charged-particle multiplicity $dN_{ch}/d\eta$ ($|\eta| < 0.5$) dependence of the yield ratio $N_t \times N_p/N_d^2$ in Au+Au collisions at $\sqrt{s_{NN}}$ = 7.7 - 200 GeV. The data from each collision energy presented in the figure include four centrality bins: 0%-10%, 10%-20%, 20%-40%, and 40%-80%, in addition, a single 0%-20% centrality bin is also presented for 54.4 GeV. It is observed that the yield ratio $N_t \times N_p/N_d^2$ shows a decreasing trend with increasing charged-particle multiplicity $dN_{ch}/d\eta$ and exhibits a scaling behavior. The shaded bands in Fig. 3 are the corresponding results from the calculations of hadronic transport AMPT and MUSIC+UrQMD hybrid models [52]. MUSIC is a (3+1)D viscous hydrodynamics model [79, 80], which conserves both energy-momentum and baryon number and is used to describe the dynamical evolution of the QGP. To provide a reliable baseline, neither critical point nor first-order phase transition is included in the AMPT and MUSIC+UrQMD hybrid model calcula-
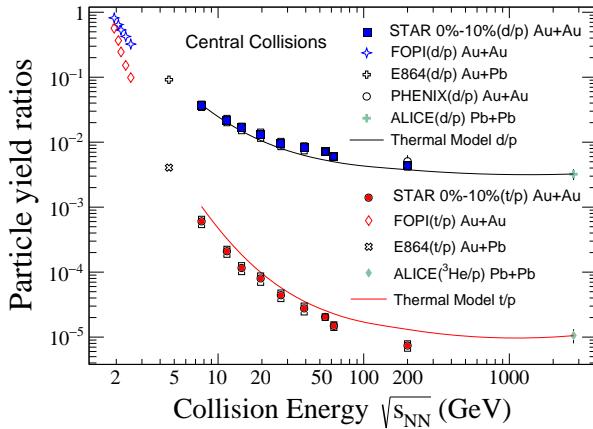
FIG. 2. Collision energy dependence of the mid-rapidity ratios N_d/N_p (blue solid squares) and N_t/N_p (red solid circles) from the top 0%-10% central Au+Au collisions. Statistical and systematic uncertainties are shown as vertical lines and brackets, respectively. For comparison, results from FOPI [73], E864 [20], PHENIX [74, 75], and ALICE [27] are also shown. The lines are results from the thermal model using chemical freeze-out conditions from Ref. [77, 78]


FIG. 3. The yield ratio $N_t \times N_p/N_d^2$ as a function of charged-particle multiplicity $dN_{ch}/d\eta$ ($|\eta| < 0.5$) in Au+Au collisions at $\sqrt{s_{NN}} = 7.7$ – 200 GeV for 0%-10%, 10%-20%, 20%-40%, and 40%-80% centralities. Statistical and systematic uncertainties are shown as vertical lines and brackets, respectively. The black dot-dashed line denotes the coalescence-inspired fit. The open diamond denotes the yield ratio of 0%-20% central Au+Au collisions at $\sqrt{s_{NN}} = 54.4$ GeV. The red shaded vertical band on the right side of the figure represents the multiplicity independent systematic uncertainties on these ratios. The significance of the deviation relative to the fit is shown in the lower panel. The results calculated from thermal model are shown as the blue long-dashed line. Calculations from AMPT and MU-SIC+UrQMD hybrid models [51, 52] are shown as shaded bands.

tions. These two models are employed to generate the nucleon phase space at kinetic freeze-out, when light nuclei are formed via nucleon coalescence. It is found that the overall trend of the experimental data is well described by the model calculations. The light blue dashed line is the result calculated from the thermal model at chemical freeze-out [77, 78] for central Au+Au collisions, which overestimates the experimental data by more than a factor of two at $dN_{ch}/d\eta \sim 600$. As discussed in Ref. [50], this overestimation could be due to the effects of hadronic re-scatterings during hadronic expansion, which reduce the triton and helium-3 yields by about a factor of 1.8 from their initial values given by thermal model. However, this cannot explain the agreement between the thermal model calculations and the $N_{3_{He}} \times N_p/N_d^2$ ratio from central Pb+Pb collisions at $\sqrt{s_{NN}} = 2.76$ TeV where $dN_{ch}/d\eta \sim 1100$ [27, 37]. Obviously, further investigations are needed to understand the discrepancy.

The black dot-dashed line is a fit to the data based on the coalescence model. As discussed in Ref. [52], assuming a thermal equilibrated and static spherical Gaussian nucleon source, one can obtain the fit function as:

$$\frac{N_t \times N_p}{N_d^2} = p_0 \times \left(\frac{R^2 + \frac{2}{3}r_d^2}{R^2 + \frac{1}{2}r_t^2} \right)^3, \qquad (1)$$

where $R = p_1 \times (dN_{ch}/d\eta)^{1/3}$ denotes the radius of the spherical nucleon emission source. $r_d = 1.96$ fm and $r_t = 1.59$ fm are the nucleonic point root-mean-square radius of deuteron and triton [81], respectively. p_0 and p_1 are the two fitting parameters where the best fit values are 0.37 ± 0.008 and 0.75 ± 0.04, respectively. At small values of $dN_{ch}/d\eta$, when the system size is comparable to the size of light nuclei, the yield ratio shows a rapid increase with decreasing $dN_{ch}/d\eta$, while it saturates at large charged-particle multiplicity. The general trend of the yield ratio $N_t \times N_p/N_d^2$ is driven by the in-

terplay between the finite size of light nuclei and the overall size of the fireball created in heavy-ion collisions. This provides strong evidence that nucleon coalescence is the correct formation mechanism to describe the light nuclei production in such collisions. If we use the coalescence-inspired fit as the baseline, the lower panel of the Fig. 3 shows that most of the measurements are within significance of 2σ from the coalescence baseline, except there are enhancements observed for the yield ratios in the 0%-10% most central Au+Au collisions at $\sqrt{s_{NN}} = 19.6$ and 27 GeV with significance of 2.3σ and 3.4σ, respectively, and for a combined significance of 4.1σ, as shown in the lower panel of Fig. 3. The yield ratio of 0%-20% central Au+Au collisions at 54.4 GeV is also shown in Fig. 3 as an open diamond. It agrees with the coalescence baseline at the same value of $dN_{ch}/d\eta$ as those data points from central collisions at $\sqrt{s_{NN}} = 19.6$ and 27 GeV. Therefore, the observed enhancement may be driven by the baryon density rather than the overall size of the system which is proportional to the charged-particle density $dN_{ch}/d\eta$. However, whether the enhancements are due to critical behavior requires further dynamical modeling of heavy-ion collisions with a realistic equation of state.

Figure 4 shows the energy dependence of the yield ratio
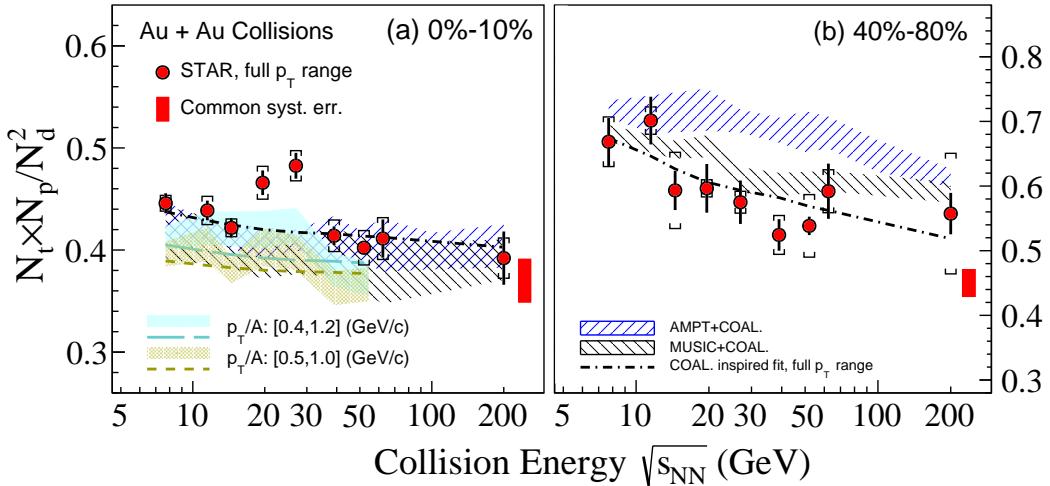
FIG. 4. Collision energy, centrality, and p_T dependence of the yield ratio $N_t \times N_p/N_d^2$ in Au+Au collisions at RHIC. Solid circles are the results from 0%-10% central (left panel) and 40%-80% peripheral (right panel) collisions. Colored-bands in panel (a) denote p_T acceptance dependence, for which the statistical and systematic uncertainties are added in quadrature. Red solid circles are the final results with extrapolation to the full p_T range. Statistical and systematic uncertainties are shown as bars and brackets, respectively. Red vertical bands on the right side of panels represent the common systematic uncertainties. Dashed lines are the coalescence baselines obtained from the coalescence-inspired fit. Shaded areas denote the calculations from hadronic transport AMPT and MUSIC+UrQMD hybrid models [52].

$N_t \times N_p/N_d^2$ at mid-rapidity in central (0%-10%) and peripheral (40%-80%) Au+Au collisions at $\sqrt{s_{NN}}$ = 7.7 - 200 GeV. For comparison, the coalescence baselines obtained by fitting the $dN_{ch}/d\eta$ dependence of the yield ratio as shown in Fig. 3 and the calculations of AMPT, MUSIC+UrQMD hybrid models are displayed in Fig. 4. For the 0%-10% most central Au+Au collisions, the yield ratios are consistent with the coalescence baseline and model calculations, except for the enhancements of the yield ratios to coalescence baseline with a significance of 2.3σ and 3.4σ observed at $\sqrt{s_{NN}}$ = 19.6 and 27 GeV, respectively. The colored-bands in panel (a) denote the yield ratios, in which the proton, deuteron, and triton yields are obtained from the commonly measured p_T/A range without any extrapolation. The enhancements and the significance of the measurements decrease with smaller p_T acceptance in the region of interest. The combined (19.6 and 27 GeV) significance of enhancements to the corresponding coalescence baselines for $0.5 \leq p_T/A \leq 1.0$ GeV/c, $0.4 \leq p_T/A \leq 1.2$ GeV/c, and the full p_T/A range are 1.6σ, 2.5σ, and 4.1σ, respectively. In the model calculations, the physics of the critical point or first-order phase transition are not included. Therefore, the non-monotonic behavior observed in the energy dependence of the yield ratio $N_t \times N_p/N_d^2$ from 0%-10% central Au+Au collisions may be due to the enhanced baryon density fluctuations induced by the critical point or first-order phase transition in heavy-ion collisions. The right panel of Fig. 4 shows the energy dependence of the yield ratio in peripheral (40%-80%) Au+Au collisions. Within uncertainties, the experimental data can be well described by the coalescence baseline (black-dashed line) whereas the calculations from AMPT and MUSIC+UrQMD hybrid models overestimate the data.

In summary, we present the measurement of triton produc-

tion and the compound yield ratio $N_t \times N_p/N_d^2$ in Au+Au collisions at $\sqrt{s_{NN}}$ = 7.7 – 200 GeV measured by the STAR experiment at RHIC. The yield ratio monotonically decreases with increasing charged-particle multiplicity ($dN_{ch}/d\eta$) and exhibits a scaling behavior, which is explained by the formation of deuteron and triton via nucleon coalescence. On the other hand, the thermal model overestimates the triton over proton yield ratio N_t/N_p and the $N_t \times N_p/N_d^2$ ratio at RHIC energies. This overestimation could indicate that the effects of hadronic re-scatterings during hadronic expansion play important role for light nuclei production in heavy-ion collisions. In the 0%-10% most central Au+Au collisions at $\sqrt{s_{NN}}$ = 19.6 and 27 GeV, the yield ratio shows enhancements relative to the coalescence baseline with a significance of 2.3σ and 3.4σ, respectively, and a combined significance of 4.1σ. The significance of the measurement decreases with reduced p_T range. This suggests that the possible enhancement may have a strong dependence on the p_T acceptance. In peripheral collisions, similar to data, model calculations have a smooth decreasing trend as a function of energy. Further detailed calculations from dynamical modeling of heavy-ion collisions with a realistic equation of state are required to determine whether the enhancements are due to large baryon density fluctuations induced by critical point. The systematic measurements of light nuclei yields and their ratios over a broad energy range provide important insights into the production dynamics of light nuclei and our understanding of the QCD phase diagram.

[1] K. Rajagopal and F. Wilczek, [arXiv:hep-ph/0011333 [hep-ph]].

[2] M. M. Aggarwal et al. [STAR], [arXiv:1007.2613 [nucl-ex]].

[3] Y. Aoki, G. Endrodi, Z. Fodor, S. D. Katz and K. K. Szabo, Nature **443**, 675-678 (2006)

[4] A. Bazavov et al. [HotQCD], Phys. Lett. B **795**, 15-21 (2019)

[5] S. Ejiri, Phys. Rev. D **78**, 074507 (2008)

[6] C. S. Fischer, Prog. Part. Nucl. Phys. **105**, 1-60 (2019)

[7] W. j. Fu, J. M. Pawlowski and F. Rennecke, Phys. Rev. D **101**, no.5, 054032 (2020)

[8] F. Gao and J. M. Pawlowski, Phys. Lett. B **820**, 136584 (2021)

[9] A. M. Halasz, A. D. Jackson, R. E. Shrock, M. A. Stephanov and J. J. M. Verbaarschot, Phys. Rev. D **58**, 096007 (1998)

[10] M. A. Stephanov, Prog. Theor. Phys. Suppl. **153**, 139-156 (2004)

[11] K. Fukushima and T. Hatsuda, Rept. Prog. Phys. **74**, 014001 (2011)

[12] S. Gupta, X. Luo, B. Mohanty, H. G. Ritter and N. Xu, Science **332**, 1525-1528 (2011)

[13] L. Adamczyk et al. [STAR], Phys. Rev. Lett. **112**, 032302 (2014)

[14] A. Bzdak, S. Esumi, V. Koch, J. Liao, M. Stephanov and N. Xu, Phys. Rept. **853**, 1-87 (2020)

[15] X. Luo and N. Xu, Nucl. Sci. Tech. **28**, no.8, 112 (2017)

[16] J. Adam et al. [STAR], Phys. Rev. Lett. **126**, no.9, 092301 (2021)

[17] M. Abdallah et al. [STAR], Phys. Rev. C **104**, no.2, 024902 (2021)

[18] V. T. Cocconi, T. Fazzini, G. Fidecaro, M. Legros, N. H. Lipman and A. W. Merrison, Phys. Rev. Lett. **5**, 19-21 (1960)

[19] J. Barrette et al. [E814], Phys. Rev. C **50**, 1077-1084 (1994)

[20] T. A. Armstrong et al. [E864], Phys. Rev. C **61**, 064908 (2000)

[21] S. Albergo, R. Bellwied, M. Bennett, B. Bonner, H. Caines, W. Christie, S. Costa, H. J. Crawford, M. Cronqvist and R. Debbe, et al. Phys. Rev. C **65**, 034907 (2002)

[22] W. Reisdorf et al. [FOPI], Nucl. Phys. A **848**, 366-427 (2010)

[23] T. Anticic et al. [NA49], Phys. Rev. C **94**, no.4, 044906 (2016)

[24] L. Adamczyk et al. [STAR], Phys. Rev. C **94**, no.3, 034908 (2016)

[25] J. Chen, D. Keane, Y. G. Ma, A. Tang and Z. Xu, Phys. Rept. **760**, 1-39 (2018)

[26] J. Adam et al. [STAR], Phys. Rev. C **99**, no.6, 064905 (2019)

[27] J. Adam et al. [ALICE], Phys. Rev. C **93**, no.2, 024917 (2016)

[28] S. Acharya et al. [ALICE], Phys. Rev. C **97**, no.2, 024615 (2018)

[29] L. P. Csernai and J. I. Kapusta, Phys. Rept. **131**, 223-318 (1986)

[30] C. B. Dover, U. W. Heinz, E. Schnedermann and J. Zimanyi, Phys. Rev. C **44**, 1636-1654 (1991)

[31] R. Scheibl and U. W. Heinz, Phys. Rev. C **59**, 1585-1602 (1999)

[32] Y. Oh, Z. W. Lin and C. M. Ko, Phys. Rev. C **80**, 064902 (2009)

[33] J. Steinheimer, K. Gudima, A. Botvina, I. Mishustin, M. Bleicher and H. Stocker, Phys. Lett. B **714**, 85-91 (2012)

[34] W. Zhao, L. Zhu, H. Zheng, C. M. Ko and H. Song, Phys. Rev. C **98**, no.5, 054905 (2018)

[35] D. Oliinychenko, L. G. Pang, H. Elfner and V. Koch, Phys. Rev. C **99**, no.4, 044907 (2019)

[36] V. Vovchenko, K. Gallmeister, J. Schaffner-Bielich and C. Greiner, Phys. Lett. B **800**, 135131 (2020)

[37] D. Oliinychenko, Nucl. Phys. A **1005**, 121754 (2021)

[38] W. Zhao, C. Shen, C. M. Ko, Q. Liu and H. Song, Phys. Rev. C **102**, no.4, 044912 (2020)

[39] K. J. Sun, R. Wang, C. M. Ko, Y. G. Ma and C. Shen,

[40] J. Staudenmaier, D. Oliinychenko, J. M. Torres-Rincon and H. Elfner, Phys. Rev. C **104**, no.3, 034908 (2021)

[41] D. Oliinychenko, C. Shen and V. Koch, Phys. Rev. C **103**, no.3, 034913 (2021)

[42] P. Hillmann, K. Käfer, J. Steinheimer, V. Vovchenko and M. Bleicher, J. Phys. G **49**, no.5, 055107 (2022)

[43] X. Y. Zhao, Y. T. Feng, F. L. Shao, R. Q. Wang and J. Song, Phys. Rev. C **105**, 054908 (2022)

[44] A. Z. Mekjian, Phys. Rev. C **17**, 1051-1070 (1978)

[45] A. Andronic, P. Braun-Munzinger, J. Stachel and H. Stocker, Phys. Lett. B **697**, 203-207 (2011)

[46] H. Sato and K. Yazaki, Phys. Lett. B **98**, 153-157 (1981)

[47] A. Andronic, P. Braun-Munzinger, K. Redlich and J. Stachel, Nature **561**, no.7723, 321-330 (2018)

[48] P. Braun-Munzinger and B. Dönigus, Nucl. Phys. A **987**, 144-201 (2019)

[49] T. Neidig, K. Gallmeister, C. Greiner, M. Bleicher and V. Vovchenko, Phys. Lett. B **827**, 136891 (2022)

[50] K. J. Sun, R. Wang, C. M. Ko, Y. G. Ma and C. Shen, [arXiv:2207.12532 [nucl-th]].

[51] K. J. Sun, C. M. Ko and B. Dönigus, Phys. Lett. B **792**, 132-137 (2019)

[52] W. Zhao, K. j. Sun, C. M. Ko and X. Luo, Phys. Lett. B **820**, 136571 (2021)

[53] K. J. Sun, L. W. Chen, C. M. Ko and Z. Xu, Phys. Lett. B **774**, 103-107 (2017)

[54] K. J. Sun, L. W. Chen, C. M. Ko, J. Pu and Z. Xu, Phys. Lett. B **781**, 499-504 (2018)

[55] E. Shuryak and J. M. Torres-Rincon, Phys. Rev. C **100**, no.2, 024903 (2019)

[56] E. Shuryak and J. M. Torres-Rincon, Phys. Rev. C **101**, no.3, 034914 (2020)

[57] E. Shuryak and J. M. Torres-Rincon, Eur. Phys. J. A **56**, no.9, 241 (2020)

[58] K. J. Sun, C. M. Ko, F. Li, J. Xu and L. W. Chen, Eur. Phys. J. A **57**, no.11, 313 (2021)

[59] K. J. Sun, F. Li and C. M. Ko, Phys. Lett. B **816**, 136258 (2021)

[60] K. J. Sun, W. H. Zhou, L. W. Chen, C. M. Ko, F. Li, R. Wang and J. Xu, [arXiv:2205.11010 [nucl-th]].

[61] V. Vovchenko, B. Dönigus and H. Stoecker, Phys. Lett. B **785**, 171-174 (2018)

[62] K. H. Ackermann *et al.* [STAR], Nucl. Instrum. Meth. A **499**, 624-632 (2003)

[63] B. I. Abelev *et al.* [STAR], Phys. Rev. C **79**, 034909 (2009)

[64] M. Anderson, J. Berkovitz, W. Betts, R. Bossingham, F. Bieser, R. Brown, M. Burks, M. Calderon de la Barca Sanchez, D. A. Cebra and M. G. Cherney, *et al.* Nucl. Instrum. Meth. A **499**, 659-678 (2003)

[65] W. J. Llope, Nucl. Instrum. Meth. B **241**, 306-310 (2005)

[66] C. Adler *et al.* [STAR], Phys. Rev. Lett. **87**, 262301 (2001) [erratum: Phys. Rev. Lett. **87**, 279902 (2001)]

[67] E. Schnedermann, J. Sollfrank and U. W. Heinz, Phys. Rev. C **48**, 2462-2475 (1993)

[68] B. I. Abelev *et al.* [STAR], Phys. Rev. Lett. **97**, 152301 (2006)

[69] L. Adamczyk *et al.* [STAR], Phys. Rev. C **96**, no.4, 044904 (2017)

[70] B. I. Abelev *et al.* [STAR], Phys. Rev. C **79**, 034909 (2009)

[71] J. Adam *et al.* [STAR], Phys. Rev. C **102**, no.3, 034909 (2020)

[72] L. Adamczyk *et al.* [STAR], Phys. Rev. Lett. **121**, no.3, 032301 (2018)

[73] W. Reisdorf *et al.* [FOPI], Nucl. Phys. A **781**, 459-508 (2007)

[74] S. S. Adler *et al.* [PHENIX], Phys. Rev. Lett. **94**, 122302 (2005)

[75] S. S. Adler *et al.* [PHENIX], Phys. Rev. C **69**, 034909 (2004)

[76] V. Vovchenko and H. Stoecker, Comput. Phys. Commun. **244**, 295-310 (2019)

[77] V. Vovchenko, V. V. Begun and M. I. Gorenstein, Phys. Rev. C **93**, no.6, 064906 (2016)

[78] V. Vovchenko, B. Dönigus, B. Kardan, M. Lorenz and H. Stoecker, Phys. Lett. **B**, 135746 (2020)

[79] C. Shen and B. Schenke, Phys. Rev. C **97**, no.2, 024907 (2018)

[80] G. S. Denicol, C. Gale, S. Jeon, A. Monnai, B. Schenke and C. Shen, Phys. Rev. C **98**, no.3, 034916 (2018)

[81] G. Ropke, Phys. Rev. C **79**, 014002 (2009)

I. SUPPLEMENTAL MATERIAL

A. Supplement to Beam Energy Dependence of Triton Production and Yield Ratio ($N_t \times N_p/N_d^2$) in Au+Au Collisions at RHIC

In heavy-ion collisions, one of the main production sources of the (anti)protons is the weak decay of strange baryons and their anti-particles, such as Λ, Σ^+, Ξ^0, Ξ^-, Ω^-. The corresponding decay channels and branching ratios are [1]

$$\Lambda \longrightarrow p + \pi^-, \text{ branching ratio} = 63.9\%$$
$$\Sigma^+ \longrightarrow p + \pi^0, \text{ branching ratio} = 51.57\%$$
$$\Xi^- \longrightarrow \Lambda + \pi^-, \text{ branching ratio} = 99.887\%$$
$$\Xi^0 \longrightarrow \Lambda + \pi^0, \text{ branching ratio} = 99.524\%$$
$$\Omega^- \longrightarrow \Lambda + K^-, \text{ branching ratio} = 67.8\%$$

Usually, the primordial yields of (anti)protons are more commonly used to study the properties of the hot dense medium created in heavy-ion collisions. Therefore, those (anti)protons from the weak decay contributions need to be subtracted from their inclusive yields.
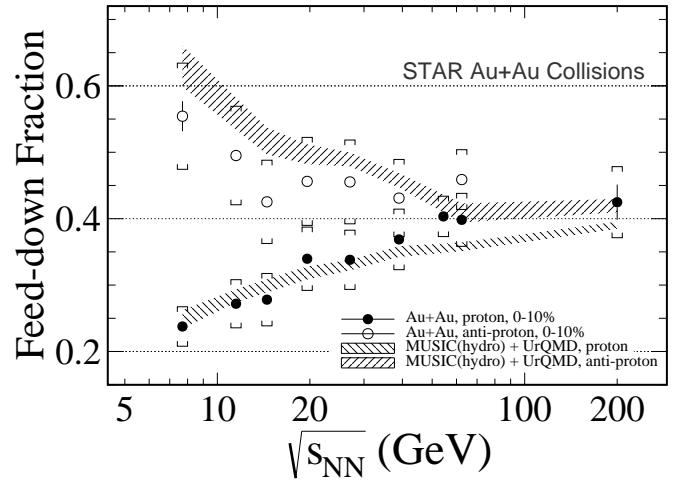
FIG. 5. The energy dependence of the weak decay feed-down fraction of proton yields at mid-rapidity estimated from the data-driven method. The black-filled circles and the black-open circles are the results of protons and antiprotons, respectively. The black-shaded bands are the corresponding calculation from the MUSIC+UrQMD hybrid model [2].

The STAR experiment has published the inclusive yields of protons and antiprotons at mid-rapidity in Au+Au collisions at $\sqrt{s_{NN}}$ = 7.7 - 200 GeV [3–7]. In STAR, the subtractions are not done on an event-by-event basis, but by subtracting the decayed (anti)protons p_T spectra from the spectra of inclusive (anti)protons. To simulate the decay kinematics of strange baryons within real detector acceptance, the so-called Monte Carlo (MC) embedding technique is used. The MC strange baryons with flat p_T are embedded into the real data and go through a realistic GEANT detector simulation. Then, the MC strange baryons are decayed into (anti)protons based on the branching ratios. Finally, the p_T spectra of decayed (anti)protons are weighted by a factor, which is the ratio of the measured p_T spectra of strange baryons over the embedded ones. Experimentally, the p_T spectra and yields of Λ, Ξ^- and Ω^- in Au+Au collisions measured at RHIC BES-I energies have been reported in Ref. [8, 9]. As the π^0 and their decay daughters are difficult to detect at mid-rapidity in the STAR experiment, the Ξ^0 and Σ^+ are not measured. However, we assume that the Ξ^0 and Ξ^- have the same p_T spectra due to the similar mass and lifetime. In addition, based on the Σ^+/Λ ratio from thermal model, the p_T spectra of Σ^+ are obtained by multiplying the p_T spectra of Λ by a factor of 0.27, which is p_T and centrality independent. To account for the uncertainty from this assumption, a 20% relative error is added to the Σ^+ spectra. In Fig 5, we show the energy dependence of the weak decay fraction for protons and antiprotons in 0-10% central Au+Au collisions. The black-filled circles and the black-open circles are the results of protons and antiprotons, respectively. The weak decay feed-down fraction of protons decreases monotonically with decreasing collision energy whereas the results of antiproton show the opposite trend. The results calculated from the MUSIC+UrQMD hy-

brid model [2] are plotted as black-shaded bands in Fig. 5.
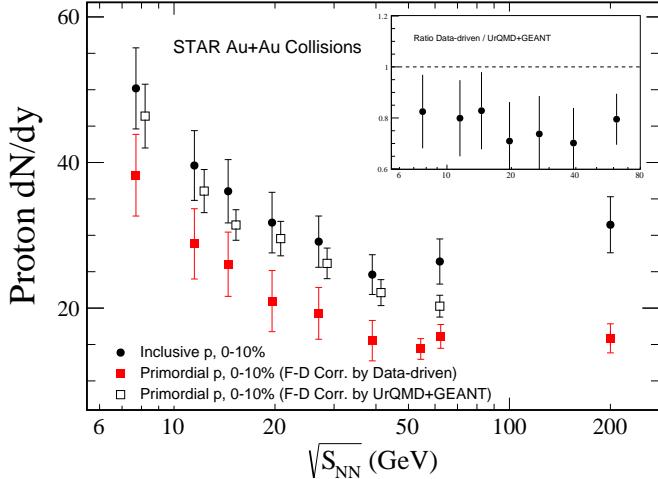
FIG. 6. The energy dependence of the primordial proton yields at mid-rapidity estimated from the data-driven method (red filled squares) and UrQMD+GEANT (open squares). The black filled circles are inclusive protons. The ratio of the data-drive method to UrQMD+GEANT method is shown in the inner panel.

It is worth pointing out that before the measurement of the strange particles, STAR has performed the weak decay feed-down corrections for protons based on UrQMD + GEANT simulation [10]. Compared with the results from the data driven method mentioned above, we find that the weak decay fractions evaluated from UrQMD+Geant simulation are underestimating the mid-rapidity primordial proton dN/dy as shown in Fig. 6. This is mainly caused by the incorrect spectra and yields of strange baryons from UrQMD. In the appendix, we have tabulated the data of primordial (anti)protons p_T spectra in Au+Au collisions at $\sqrt{s_{NN}}$ = 7.7 - 200 GeV from the data-driven method.

Another addition to the supplementary material to the article is information related to the light nuclei yield ratio. Since the ALICE collaboration has published the proton and light nuclei yield in p+p collisions at 7.0 TeV [11–13], p+Pb collisions at 5.02 TeV [14, 15] and Pb+Pb collisions at 2.76 GeV [16, 17], we calculated the corresponding light nuclei yield ratio based on these published data. The calculation results of the Thermal-FIST model also added the light nuclei ratio at μ_B = 0 MeV for different temperature [19]. As we can see from the Fig. 7, it seems that ALICE measurements are closer to the thermal model, while STAR results can be better described using coalescence model.
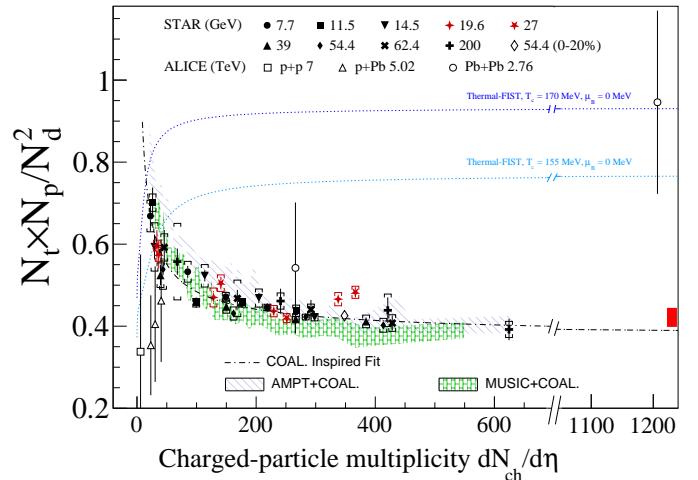
FIG. 7. The yield ratio ($N_t \times N_p/N_d^2$) as a function of charge particle multiplicity $dN_{ch}/d\eta$ in Au + Au collisions at $\sqrt{s_{NN}}$ = 7.7 - 200 GeV from STAR by solid symbols. The open diamond denotes the yield ratio of 0%-20% central Au+Au collisions at $\sqrt{s_{NN}}$ = 54.4 GeV. Statistical and systematic uncertainties are shown as vertical lines and brackets, respectively. The black dot-dashed line denotes the coalescence-inspired fit. The red shaded vertical band on the right side of the figure represents the multiplicity independence systematic uncertainties on these ratios from STAR measurements. From ALICE results: The open square is from p+p 7 TeV [11–13], the open triangle is from p+Pb 5.02 TeV [14, 15], and the open circle is from Pb+Pb 2.76 TeV [16, 17]. Statistical error and systematic error are combined shown as vertical lines. The results from a Thermal-FIST model with μ_B = 0 MeV at different temperature are shown as the blue dotted lines. Calculations from AMPT [18] and MU-SIC+UrQMD hybrid [2] models are shown as shaded blue and green bands, respectively.

Appendix A: Invariant transverse momentum (p_T) spectra of primordial protons in Au+Au collisions at $\sqrt{s_{\mathrm{NN}}}$ = 7.7 - 200 GeV.

TABLE I. Invariant p_T spectra ($\frac{1}{2\pi}\frac{d^2N}{p_T dp_T dy}\pm$stat$\pm$sys $(\mathrm{GeV}/c)^{-2}$) of primordial protons in 0-10%, 10-20% and 20-40% Au+Au collisions at $\sqrt{s_{\mathrm{NN}}}$ = 7.7 GeV.

p_T^{low}	p_T^{high}	$\frac{1}{2\pi}\frac{d^2N}{p_T dy dp_T}$		
		0-10%	10-20%	20-40%
0.40	0.45	11.86 ±0.12 ±1.95	8.53 ±6.70e-02±1.34	5.49 ±5.24e-02 ±0.81
0.45	0.50	11.15 ±0.11 ±1.41	8.14 ±6.32e-02±0.97	5.11 ±4.82e-02 ±0.58
0.50	0.55	10.45 ±0.10 ±1.12	7.66 ±6.01e-02±0.78	4.72 ±4.51e-02 ±0.45
0.55	0.60	9.80 ±9.56e-02 ±0.94	7.22 ±5.64e-02±0.67	4.29 ±4.14e-02 ±0.38
0.60	0.65	9.02 ±8.90e-02 ±0.82	6.68 ±5.15e-02±0.59	3.89 ±3.76e-02 ±0.33
0.65	0.70	8.40 ±8.19e-02 ±0.74	6.05 ±4.83e-02±0.52	3.46 ±3.42e-02 ±0.29
0.70	0.75	7.75 ±7.52e-02 ±0.66	5.52 ±4.33e-02±0.46	3.09 ±3.11e-02 ±0.25
0.75	0.80	7.10 ±6.90e-02 ±0.59	5.01 ±3.91e-02±0.41	2.78 ±2.83e-02 ±0.22
0.80	0.85	6.45 ±6.33e-02 ±0.53	4.50 ±3.58e-02±0.36	2.45 ±2.54e-02 ±0.19
0.85	0.90	5.86 ±5.77e-02 ±0.48	4.02 ±3.13e-02±0.32	2.15 ±2.28e-02 ±0.17
0.90	0.95	5.23 ±5.17e-02 ±0.42	3.56 ±2.78e-02±0.28	1.91 ±2.05e-02 ±0.15
0.95	1.0	4.67 ±4.70e-02 ±0.37	3.13 ±2.46e-02±0.25	1.64 ±1.82e-02 ±0.13
1.0	1.10	3.83 ±4.19e-02 ±0.30	2.50 ±2.49e-02±0.20	1.31 ±1.57e-02 ±0.10
1.10	1.20	2.93 ±3.29e-02 ±0.23	1.89 ±1.89e-02±0.15	0.97 ±1.22e-02 ±7.40e-02
1.20	1.30	2.24 ±2.59e-02 ±0.18	1.38 ±1.38e-02±0.11	0.71 ±9.36e-03 ±5.44e-02
1.30	1.40	1.66 ±2.02e-02 ±0.13	0.99 ±1.02e-02±8.01e-02	0.50 ±7.21e-03 ±3.98e-02
1.40	1.50	1.18 ±1.57e-02 ±0.10	0.70 ±7.35e-03±6.05e-02	0.35 ±5.55e-03 ±2.99e-02
1.50	1.60	0.84 ±1.22e-02 ±8.22e-02	0.50 ±5.46e-03±4.88e-02	0.25±4.33e-03 ±2.40e-02
1.60	1.70	0.59 ±9.63e-03 ±7.09e-02	0.34 ±4.0e-03±4.08e-02	0.17 ±3.35e-03 ±1.98e-02
1.70	1.80	0.41 ±7.56e-03 ±4.84e-02	0.22 ±2.93e-03±2.67e-02	0.11±2.62e-03 ±1.32e-02
1.80	1.90	0.28 ±6.00e-03 ±3.29e-02	0.15 ±2.18e-03±1.79e-02	7.69e-02±2.05e-03 ±8.93e-03
1.90	2.0	0.19 ±4.78e-03 ±2.23e-02	9.61e-02 ±1.62e-03±1.14e-02	5.01e-02±1.59e-03 ±5.79e-03

TABLE II. Invariant p_T spectra ($\frac{1}{2\pi}\frac{d^2N}{p_T dp_T dy}\pm$stat$\pm$sys $(\mathrm{GeV}/c)^{-2}$) of primordial protons in 40-60% and 60-80% Au+Au collisions at $\sqrt{s_{\mathrm{NN}}}$ = 7.7 GeV.

p_T^{low}	p_T^{high}	$\frac{1}{2\pi}\frac{d^2N}{p_T dy dp_T}$	p_T^{low}	p_T^{high}	$\frac{1}{2\pi}\frac{d^2N}{p_T dy dp_T}$
		40-60%			60-80%
0.40	0.45	2.57 ±3.48e-02 ±0.36	0.40	0.45	0.87 ±1.79e-02 ±0.12
0.45	0.50	2.29 ±3.17e-02 ±0.25	0.45	0.50	0.75 ±1.60e-02 ±7.56e-02
0.50	0.55	2.04 ±2.84e-02 ±0.19	0.50	0.55	0.63 ±1.44e-02 ±5.44e-02
0.55	0.60	1.78 ±2.56e-02 ±0.15	0.55	0.60	0.54 ±1.33e-02 ±4.25e-02
0.60	0.65	1.58 ±2.31e-02 ±0.13	0.60	0.70	0.41 ±1.0e-02 ±3.04e-02
0.65	0.70	1.36 ±2.05e-02 ±0.11	0.70	0.80	0.29 ±7.72e-03 ±2.09e-02
0.70	0.75	1.18 ±1.85e-02 ±9.14e-02	0.80	0.90	0.20 ±6.02e-03 ±1.45e-02
0.75	0.80	1.03 ±1.65e-02 ±7.90e-02	0.90	1.0	0.14 ±4.67e-03 ±9.91e-03
0.80	0.85	0.89 ±1.47e-02 ±6.77e-02	1.0	1.10	9.46e-02 ±3.65e-03 ±6.71e-03
0.85	0.90	0.77 ±1.29e-02 ±5.77e-02	1.10	1.20	6.32e-02 ±2.89e-03 ±4.48e-03
0.90	0.95	0.65 ±1.15e-02 ±4.88e-02	1.20	1.30	4.35e-02 ±2.25e-03 ±3.10e-03
0.95	1.0	0.57 ±1.03e-02 ±4.20e-02	1.30	1.40	2.68e-02 ±1.77e-03 ±1.99e-03
1.0	1.10	0.43 ±8.30e-03 ±3.15e-02	1.40	1.50	1.63e-02 ±1.33e-03 ±1.32e-03
1.10	1.20	0.31 ±6.36e-03 ±2.27e-02	1.50	1.60	1.02e-02 ±1.04e-03 ±9.61e-04
1.20	1.30	0.22 ±4.92e-03 ±1.61e-02	1.60	1.70	6.85e-03 ±7.85e-04± 7.89e-04
1.30	1.40	0.15 ±3.73e-03 ±1.12e-02	1.70	1.80	3.96e-03 ±5.73e-04± 4.91e-04
1.40	1.50	0.10 ±2.90e-03 ±8.27e-03	1.80	1.90	3.16e-03 ±5.21e-04± 3.91e-04
1.50	1.60	6.61e-02 ±2.23e-03 ±6.24e-03	1.90	2.0	1.74e-03 ±5.59e-04± 2.75e-04
1.60	1.70	4.40e-02 ±1.73e-03 ±5.11e-03			
1.70	1.80	2.84e-02 ±1.33e-03 ±3.29e-03			
1.80	1.90	1.71e-02 ±1.0e-03 ±1.99e-03			
1.90	2.0	1.12e-02 ±7.98e-04 ±1.30e-03			

TABLE III. Invariant p_T spectra ($\frac{1}{2\pi}\frac{d^2N}{p_T dp_T dy}\pm$stat$\pm$sys (GeV/c)$^{-2}$) of primordial protons in 0-10%, 10-20% and 20-40% Au+Au collisions at $\sqrt{s_{NN}}$ = 11.5 GeV.

p_T^{low}	p_T^{high}	$\frac{1}{2\pi}\frac{d^2N}{p_T dy dp_T}$		
		0-10%	10-20%	20-40%
0.40	0.45	9.0 ±7.12e-02 ±1.63	6.16 ±4.14e-02 ±1.20	3.92 ±3.35e-02 ±0.70
0.45	0.50	8.57 ±6.65e-02 ±1.25	5.81 ±3.96e-02 ±0.85	3.58 ±3.06e-02 ±0.52
0.50	0.55	8.10 ±6.19e-02 ±1.05	5.45 ±3.75e-02 ±0.71	3.27 ±2.83e-02 ±0.42
0.55	0.60	7.65 ±5.79e-02 ±0.92	5.07 ±3.47e-02 ±0.62	2.99 ±2.61e-02 ±0.36
0.60	0.65	7.10 ±5.35e-02 ±0.83	4.70 ±3.23e-02 ±0.55	2.68 ±2.39e-02 ±0.32
0.65	0.70	6.58 ±4.95e-02 ±0.75	4.28 ±2.95e-02 ±0.49	2.42 ±2.19e-02 ±0.28
0.70	0.75	6.02 ±4.57e-02 ±0.67	3.93 ±2.69e-02 ±0.44	2.16 ±1.96e-02 ±0.25
0.75	0.80	5.53 ±4.18e-02 ±0.61	3.54 ±2.46e-02 ±0.40	1.94 ±1.80e-02 ±0.22
0.80	0.85	5.02 ±3.80e-02 ±0.55	3.22 ±2.22e-02 ±0.35	1.71 ±1.62e-02 ±0.19
0.85	0.90	4.51 ±3.48e-02 ±0.48	2.87 ±1.98e-02 ±0.31	1.51 ±1.44e-02 ±0.17
0.90	0.95	4.07 ±3.17e-02 ±0.43	2.57 ±1.77e-02 ±0.28	1.34 ±1.29e-02 ±0.15
0.95	1.0	3.64 ±2.86e-02 ±0.38	2.27 ±1.56e-02 ±0.24	1.17 ±1.16e-02 ±0.13
1.0	1.10	2.89 ±2.58e-02 ±0.31	1.81 ±1.63e-02 ±0.19	0.93 ±1.05e-02 ±0.10
1.10	1.20	2.20 ±2.05e-02 ±0.23	1.38 ±1.25e-02 ±0.15	0.70 ±8.18e-03 ±7.44e-02
1.20	1.30	1.66 ±1.61e-02 ±0.17	1.03 ±9.53e-03 ±0.11	0.52 ±6.31e-03 ±5.47e-02
1.30	1.40	1.22 ±1.26e-02 ±0.13	0.75 ±7.08e-03 ±8.04e-02	0.38 ±4.86e-03 ±4.03e-02
1.40	1.50	0.87 ±9.80e-03 ±9.77e-02	0.55 ±5.26e-03 ±6.12e-02	0.27 ±3.75e-03 ±3.01e-02
1.50	1.60	0.63 ±7.71e-03 ±7.66e-02	0.39 ±3.92e-03 ±4.75e-02	0.19 ±2.91e-03 ±2.32e-02
1.60	1.70	0.43 ±5.98e-03 ±6.23e-02	0.27 ±2.90e-03 ±3.92e-02	0.13 ±2.27e-03 ±1.88e-02
1.70	1.80	0.30 ±4.67e-03 ±4.29e-02	0.19 ±2.18e-03 ±2.69e-02	9.23e-02 ±1.79e-03 ±1.29e-02
1.80	1.90	0.21 ±3.68e-03 ±2.94e-02	0.13 ±1.65e-03 ±1.85e-02	6.27e-02 ±1.40e-03 ±8.66e-03
1.90	2.0	0.14 ±2.93e-03 ±2.0e-02	9.02e-02 ±1.26e-03 ±1.25e-02	4.53e-02 ±1.13e-03 ±6.14e-03

TABLE IV. Invariant p_T spectra ($\frac{1}{2\pi}\frac{d^2N}{p_T dp_T dy}\pm$stat$\pm$sys (GeV/c)$^{-2}$) of primordial protons in 40-60% and 60-80% Au+Au collisions at $\sqrt{s_{NN}}$ = 11.5 GeV.

p_T^{low}	p_T^{high}	$\frac{1}{2\pi}\frac{d^2N}{p_T dy dp_T}$	
		40-60%	60-80%
0.40	0.45	1.79 ±2.10e-02±0.30	0.55±1.12e-02 ±9.46e-02
0.45	0.50	1.61 ±1.92e-02±0.22	0.48±9.98e-03 ±6.64e-02
0.50	0.55	1.43 ±1.79e-02±0.18	0.42±9.05e-03 ±5.14e-02
0.55	0.60	1.26 ±1.64e-02±0.15	0.35±8.02e-03 ±4.14e-02
0.60	0.65	1.10 ±1.46e-02±0.13	0.30±7.17e-03 ±3.46e-02
0.65	0.70	0.95 ±1.32e-02±0.11	0.26±6.39e-03 ±2.90e-02
0.70	0.75	0.83 ±1.19e-02±9.40e-02	0.21±5.68e-03 ±2.39e-02
0.75	0.80	0.71 ±1.06e-02±8.02e-02	0.18±4.94e-03 ±2.0e-02
0.80	0.85	0.61 ±9.46e-03±6.88e-02	0.15±4.41e-03 ±1.69e-02
0.85	0.90	0.53 ±8.43e-03±5.86e-02	0.12±3.86e-03 ±1.37e-02
0.90	0.95	0.44 ±7.53e-03±4.94e-02	0.10±3.43e-03 ±1.15e-02
0.95	1.0	0.38 ±6.63e-03±4.24e-02	8.61e-02±3.03e-03 ±9.48e-03
1.0	1.10	0.29 ±5.87e-03±3.24e-02	6.50e-02±2.36e-03 ±7.10e-03
1.10	1.20	0.21 ±4.45e-03±2.33e-02	4.43e-02±1.82e-03 ±4.79e-03
1.20	1.30	0.15 ±3.44e-03±1.64e-02	3.02e-02±1.43e-03 ±3.24e-03
1.30	1.40	0.11 ±2.61e-03±1.17e-02	1.95e-02±1.07e-03 ±2.13e-03
1.40	1.50	7.36e-02 ±1.98e-03±8.43e-03	1.39e-02±8.45e-04 ±1.54e-03
1.50	1.60	4.86e-02 ±1.48e-03±6.13e-03	9.11e-03±6.64e-04 ±1.09e-03
1.60	1.70	3.35e-02 ±1.15e-03±4.89e-03	5.70e-03±5.39e-04 ±7.96e-04
1.70	1.80	2.24e-02 ±8.66e-04±3.22e-03	3.75e-03±3.91e-04 ±5.23e-04
1.80	1.90	1.40e-02 ±6.42e-04±2.03e-03	2.45e-03±3.23e-04 ±3.37e-04
1.90	2.0	9.68e-03 ±5.03e-04±1.38e-03	1.43e-03±2.46e-04 ±2.01e-04

TABLE V. Invariant p_T spectra ($\frac{1}{2\pi}\frac{d^2N}{p_T dp_T dy}\pm$stat$\pm$sys (GeV/c)$^{-2}$) of primordial protons in 0-10%, 10-20% and 20-40% Au+Au collisions at $\sqrt{s_{NN}}$ = 14.5 GeV.

p_T^{low}	p_T^{high}	$\frac{1}{2\pi}\frac{d^2N}{p_T dy dp_T}$		
		0-10%	10-20%	20-40%
0.50	0.55	6.81 ±6.20e-02 ±1.17	4.55 ±4.33e-02 ±0.76	2.45 ±2.75e-02 ±0.41
0.55	0.60	6.38 ±5.87e-02 ±1.06	4.34 ±4.10e-02 ±0.71	2.42 ±2.50e-02 ±0.39
0.60	0.65	5.95 ±5.54e-02 ±0.97	4.11 ±3.81e-02 ±0.66	2.24 ±2.32e-02 ±0.36
0.65	0.70	5.52 ±5.22e-02 ±0.88	3.75 ±3.52e-02 ±0.60	2.07 ±2.07e-02 ±0.32
0.70	0.75	4.99 ±4.80e-02 ±0.79	3.52 ±3.24e-02 ±0.55	1.89 ±1.88e-02 ±0.29
0.75	0.80	4.70 ±4.49e-02 ±0.73	3.26 ±2.96e-02 ±0.50	1.72 ±1.69e-02 ±0.26
0.80	0.85	4.17 ±4.07e-02 ±0.65	2.95 ±2.68e-02 ±0.45	1.59 ±1.54e-02 ±0.24
0.85	0.90	3.70 ±3.69e-02 ±0.57	2.53 ±2.37e-02 ±0.39	1.38 ±1.37e-02 ±0.21
0.90	0.95	3.40 ±3.37e-02 ±0.52	2.33 ±2.20e-02 ±0.35	1.24 ±1.23e-02 ±0.18
0.95	1.0	2.94 ±3.08e-02 ±0.45	1.97 ±1.91e-02 ±0.30	1.05 ±1.10e-02 ±0.16
1.0	1.10	2.49 ±3.20e-02 ±0.37	1.63 ±2.19e-02 ±0.24	0.84 ±1.11e-02 ±0.12
1.10	1.20	1.94 ±2.50e-02 ±0.29	1.25 ±1.67e-02 ±0.18	0.63 ±8.52e-03 ±9.09e-02
1.20	1.30	1.49 ±1.92e-02 ±0.22	0.95 ±1.25e-02 ±0.14	0.47 ±6.48e-03 ±6.72e-02
1.30	1.40	1.11 ±1.45e-02 ±0.16	0.71 ±9.21e-03 ±0.10	0.35 ±4.88e-03 ±4.86e-02
1.40	1.50	0.83 ±1.09e-02 ±0.12	0.51 ±6.78e-03 ±7.19e-02	0.25 ±3.72e-03 ±3.48e-02
1.50	1.60	0.50 ±8.20e-03 ±8.23e-02	0.37 ±4.89e-03 ±5.15e-02	0.18 ±2.81e-03 ±2.46e-02
1.60	1.70	0.43 ±6.17e-03 ±5.85e-02	0.27 ±3.50e-03 ±3.66e-02	0.13 ±2.11e-03 ±1.73e-02
1.70	1.80	0.30 ±4.70e-03 ±4.09e-02	0.19 ±2.58e-03 ±2.56e-02	8.91e-02 ±1.61e-03 ±1.19e-02
1.80	1.90	0.21 ±3.54e-03 ±2.84e-02	0.13 ±1.86e-03 ±1.78e-02	6.32e-02 ±1.24e-03 ±8.34e-03
1.90	2.0	0.15 ±2.75e-03 ±1.98e-02	9.39e-02 ±1.35e-03 ±1.24e-02	4.36e-02 ±9.62e-04 ±5.71e-03

TABLE VI. Invariant p_T spectra ($\frac{1}{2\pi}\frac{d^2N}{p_T dp_T dy}\pm$stat$\pm$sys (GeV/c)$^{-2}$) of primordial protons in 40-60% and 60-80% Au+Au collisions at $\sqrt{s_{NN}}$ = 14.5 GeV.

p_T^{low}	p_T^{high}	$\frac{1}{2\pi}\frac{d^2N}{p_T dy dp_T}$	
		40-60%	60-80%
0.50	0.55	0.82 ±1.78e-02±0.15	0.24 ±9.06e-03±4.26e-02
0.55	0.60	0.79 ±1.61e-02±0.14	0.23 ±7.86e-03±3.75e-02
0.60	0.65	0.78 ±1.43e-02±0.13	0.22 ±6.89e-03±3.35e-02
0.65	0.70	0.75 ±1.26e-02±0.11	0.20 ±5.89e-03±2.94e-02
0.70	0.75	0.67 ±1.11e-02±0.10	0.18 ±5.03e-03±2.60e-02
0.75	0.80	0.58 ±9.97e-03±8.79e-02	0.16 ±4.80e-03±2.27e-02
0.80	0.85	0.53 ±8.91e-03±7.79e-02	0.14 ±3.87e-03±1.92e-02
0.85	0.90	0.45 ±7.76e-03±6.61e-02	0.12 ±3.47e-03±1.62e-02
0.90	0.95	0.39 ±6.90e-03±5.68e-02	0.10 ±3.03e-03±1.41e-02
0.95	1.0	0.35 ±6.10e-03±4.97e-02	8.78e-02 ±2.60e-03±1.18e-02
1.0	1.10	0.27 ±5.67e-03±3.81e-02	6.78e-02 ±2.02e-03±9.01e-03
1.10	1.20	0.20 ±4.30e-03±2.77e-02	4.72e-02 ±1.51e-03±6.19e-03
1.20	1.30	0.15 ±3.24e-03±2.0e-02	3.30e-02 ±1.19e-03±4.26e-03
1.30	1.40	0.10 ±2.38e-03±1.40e-02	2.16e-02 ±8.95e-04±2.77e-03
1.40	1.50	7.53e-02 ±1.83e-03±9.98e-03	1.41e-02 ±6.85e-04±1.80e-03
1.50	1.60	5.42e-02 ±1.39e-03±7.06e-03	8.96e-03 ±5.50e-04±1.14e-03
1.60	1.70	3.75e-02 ±1.06e-03±4.83e-03	5.65e-03 ±4.07e-04±7.16e-04
1.70	1.80	2.67e-02 ±8.42e-04±3.38e-03	3.96e-03 ±3.39e-04±4.93e-04
1.80	1.90	1.82e-02 ±6.56e-04±2.28e-03	2.37e-03 ±2.63e-04±2.96e-04
1.90	2.0	1.33e-02 ±5.48e-04±1.64e-03	1.43e-03 ±1.81e-04±1.79e-04

TABLE VII. Invariant p_T spectra ($\frac{1}{2\pi}\frac{d^2N}{p_T dp_T dy}\pm$stat$\pm$sys (GeV/c)$^{-2}$) of primordial protons in 0-10%, 10-20% and 20-40% Au+Au collisions at $\sqrt{s_{NN}}$ = 19.6 GeV.

p_T^{low}	p_T^{high}	$\frac{1}{2\pi}\frac{d^2N}{p_T dy dp_T}$		
		0-10%	10-20%	20-40%
0.40	0.45	6.41 ±5.62e-02±1.30	4.67 ±4.13e-02±0.91	2.77 ±2.54e-02 ±0.53
0.45	0.50	5.95 ±5.31e-02±0.99	4.40 ±4.01e-02±0.69	2.57 ±2.44e-02 ±0.40
0.50	0.55	5.60 ±5.11e-02±0.83	4.11 ±3.82e-02±0.58	2.41 ±2.29e-02 ±0.33
0.55	0.60	5.17 ±4.87e-02±0.72	3.79 ±3.54e-02±0.50	2.20 ±2.16e-02 ±0.29
0.60	0.65	4.88 ±4.57e-02±0.65	3.47 ±3.36e-02±0.45	1.99 ±2.02e-02 ±0.25
0.65	0.70	4.48 ±4.23e-02±0.59	3.21 ±3.10e-02±0.40	1.78 ±1.86e-02 ±0.22
0.70	0.75	4.13 ±3.93e-02±0.53	2.92 ±2.88e-02±0.36	1.59 ±1.68e-02 ±0.20
0.75	0.80	3.80 ±3.56e-02±0.48	2.66 ±2.64e-02±0.33	1.44 ±1.53e-02 ±0.18
0.80	0.90	3.23 ±4.08e-02±0.40	2.22 ±3.12e-02±0.27	1.19 ±1.71e-02 ±0.14
0.90	1.0	2.63 ±3.35e-02±0.32	1.79 ±2.50e-02±0.21	0.91 ±1.36e-02 ±0.11
1.0	1.10	2.11 ±2.66e-02±0.25	1.41 ±1.97e-02±0.16	0.71 ±1.06e-02 ±8.35e-02
1.10	1.20	1.66 ±2.08e-02±0.19	1.11 ±1.52e-02±0.13	0.54 ±8.09e-03 ±6.26e-02
1.20	1.30	1.28 ±1.61e-02±0.15	0.85 ±1.16e-02±9.65e-02	0.40 ±6.05e-03 ±4.63e-02
1.30	1.40	0.96 ±1.23e-02±0.11	0.63 ±8.66e-03±7.31e-02	0.29 ±4.48e-03 ±3.42e-02
1.40	1.50	0.71 ±9.34e-03±8.73e-02	0.47 ±6.46e-03±5.64e-02	0.21 ±3.29e-03 ±2.58e-02
1.50	1.60	0.52 ±6.95e-03±6.91e-02	0.34 ±4.65e-03±4.44e-02	0.15 ±2.42e-03 ±1.97e-02
1.60	1.70	0.37 ±5.18e-03±5.71e-02	0.25 ±3.40e-03±3.75e-02	0.10 ±1.75e-03 ±1.58e-02
1.70	1.80	0.26 ±3.90e-03±4.02e-02	0.18 ±2.48e-03±2.65e-02	6.96e-02 ±1.27e-03 ±1.07e-02
1.80	1.90	0.18 ±2.95e-03±2.81e-02	0.13 ±1.77e-03±1.87e-02	4.57e-02 ±9.22e-04 ±7.05e-03
1.90	2.0	0.13 ±2.21e-03±1.94e-02	9.04e-02 ±1.30e-03±1.33e-02	3.03e-02 ±6.60e-04 ±4.66e-03

TABLE VIII. Invariant p_T spectra ($\frac{1}{2\pi}\frac{d^2N}{p_T dp_T dy}\pm$stat$\pm$sys (GeV/c)$^{-2}$) of primordial protons in 40-60% and 60-80% Au+Au collisions at $\sqrt{s_{NN}}$ = 19.6 GeV.

p_T^{low}	p_T^{high}	$\frac{1}{2\pi}\frac{d^2N}{p_T dy dp_T}$	
		40-60%	60-80%
0.40	0.45	1.27 ±1.75e-02 ±0.24	0.44 ±7.60e-03±7.52e-02
0.45	0.50	1.16 ±1.63e-02 ±0.18	0.39 ±6.83e-03±5.37e-02
0.50	0.55	1.06 ±1.52e-02 ±0.14	0.34 ±6.30e-03±4.20e-02
0.55	0.60	0.95 ±1.38e-02 ±0.12	0.30 ±5.49e-03±3.39e-02
0.60	0.65	0.82 ±1.27e-02 ±0.10	0.25 ±5.09e-03±2.81e-02
0.65	0.70	0.71 ±1.16e-02 ±8.68e-02	0.22 ±4.53e-03±2.34e-02
0.70	0.75	0.63 ±1.0e-02 ±7.54e-02	0.19 ±3.92e-03±2.0e-02
0.75	0.80	0.55 ±8.95e-03 ±6.48e-02	0.16 ±3.54e-03±1.71e-02
0.80	0.90	0.45 ±9.65e-03 ±5.17e-02	0.12 ±3.19e-03±1.31e-02
0.90	1.0	0.33 ±7.40e-03 ±3.74e-02	8.68e-02 ±2.38e-03±9.21e-03
1.0	1.10	0.25 ±5.60e-03 ±2.74e-02	6.10e-02 ±1.83e-03±6.47e-03
1.10	1.20	0.18 ±4.10e-03 ±1.99e-02	4.41e-02 ±1.37e-03±4.61e-03
1.20	1.30	0.13 ±3.04e-03 ±1.44e-02	3.03e-02 ±1.03e-03±3.19e-03
1.30	1.40	9.27e-02 ±2.26e-03 ±1.04e-02	2.06e-02 ±7.75e-04±2.20e-03
1.40	1.50	6.61e-02 ±1.62e-03 ±7.69e-03	1.37e-02 ±5.93e-04±1.53e-03
1.50	1.60	4.63e-02 ±1.21e-03 ±5.87e-03	9.44e-03 ±4.75e-04±1.15e-03
1.60	1.70	3.21e-02 ±8.82e-04 ±4.72e-03	6.47e-03 ±3.61e-04±9.08e-04
1.70	1.80	2.19e-02 ±6.49e-04 ±3.19e-03	3.94e-03 ±2.74e-04±5.55e-04
1.80	1.90	1.51e-02 ±4.90e-04 ±2.18e-03	2.77e-03 ±2.12e-04±3.88e-04
1.90	2.0	9.89e-03 ±3.61e-04 ±1.42e-03	1.93e-03 ±1.89e-04±2.67e-04

TABLE IX. Invariant p_T spectra ($\frac{1}{2\pi}\frac{d^2N}{p_T dp_T dy}\pm$stat$\pm$sys (GeV/c)$^{-2}$) of primordial protons in 0-10%, 10-20% and 20-40% Au+Au collisions at $\sqrt{s_{NN}}$ = 27 GeV.

p_T^{low}	p_T^{high}	$\frac{1}{2\pi}\frac{d^2N}{p_T dy dp_T}$		
		0-10%	10-20%	20-40%
0.40	0.45	5.79±4.06e-02±1.17	4.22±3.19e-02±0.82	2.64±1.91e-02±0.50
0.45	0.50	5.41±3.97e-02±0.90	3.95±3.09e-02±0.63	2.42±1.80e-02±0.37
0.50	0.55	4.99±3.84e-02±0.75	3.66±2.97e-02±0.52	2.17±1.75e-02±0.30
0.55	0.60	4.59±3.65e-02±0.65	3.33±2.83e-02±0.45	1.99±1.64e-02±0.26
0.60	0.65	4.22±3.44e-02±0.58	3.03±2.65e-02±0.40	1.78±1.55e-02±0.23
0.65	0.70	3.88±3.02e-02±0.52	2.79±2.50e-02±0.36	1.60±1.43e-02±0.21
0.70	0.75	3.54±3.02e-02±0.47	2.56±2.29e-02±0.33	1.44±1.30e-02±0.18
0.75	0.80	3.30±2.81e-02±0.42	2.32±2.10e-02±0.29	1.29±1.19e-02±0.16
0.80	0.90	2.87±3.25e-02±0.36	2.01±2.56e-02±0.25	1.10±1.37e-02±0.14
0.90	1.0	2.39±2.67e-02±0.29	1.63±2.10e-02±0.20	0.87±1.10e-02±0.11
1.0	1.10	1.92±2.15e-02±0.23	1.30±1.65e-02±0.16	0.68±8.62e-03±8.18e-02
1.10	1.20	1.53±1.71e-02±0.18	1.02±1.27e-02±0.12	0.52±6.58e-03±6.18e-02
1.20	1.30	1.19±1.31e-02±0.14	0.78±9.63e-03±9.13e-02	0.39±5.03e-03±4.63e-02
1.30	1.40	0.89±1.01e-02±0.11	0.58±7.16e-03±6.91e-02	0.29±3.73e-03±3.46e-02
1.40	1.50	0.66±7.57e-03±8.26e-02	0.43±5.27e-03±5.29e-02	0.21±2.78e-03±2.64e-02
1.50	1.60	0.47±5.63e-03±6.50e-02	0.32±3.84e-03±4.23e-02	0.15±2.04e-03±2.06e-02
1.60	1.70	0.34±4.18e-03±5.47e-02	0.22±2.78e-03±3.51e-02	0.11±1.51e-03±1.72e-02
1.70	1.80	0.25±3.11e-03±3.85e-02	0.16±1.97e-03±2.50e-02	7.84e-02±1.11e-03±1.21e-02
1.80	1.90	0.18±2.33e-03±2.72e-02	0.17±1.43e-03±1.77e-02	5.58e-02±8.26e-04±8.51e-03
1.90	2.0	0.12±1.75e-03±1.90e-02	8.23e-02±1.02e-03±1.24e-02	3.99e-02±6.18e-04±5.98e-03

TABLE X. Invariant p_T spectra ($\frac{1}{2\pi}\frac{d^2N}{p_T dp_T dy}\pm$stat$\pm$sys (GeV/c)$^{-2}$) of primordial protons in 40-60% and 60-80% Au+Au collisions at $\sqrt{s_{NN}}$ = 27 GeV.

p_T^{low}	p_T^{high}	$\frac{1}{2\pi}\frac{d^2N}{p_T dy dp_T}$	
		40-60%	60-80%
0.40	0.45	1.21 ±1.32e-02±0.23	0.45±5.41e-03±7.46e-02
0.45	0.50	1.11 ±1.25e-02±0.17	0.37±4.95e-03±5.21e-02
0.50	0.55	0.98 ±1.16e-02±0.14	0.31±4.64e-03±3.98e-02
0.55	0.60	0.87 ±1.07e-02±0.11	0.28±4.13e-03±3.32e-02
0.60	0.65	0.75 ±9.75e-03±9.60e-02	0.23±3.72e-03±2.73e-02
0.65	0.70	0.66 ±8.77e-03±8.27e-02	0.19±3.31e-03±2.25e-02
0.70	0.75	0.58 ±8.01e-03±7.12e-02	0.17±2.95e-03±1.89e-02
0.75	0.80	0.51 ±7.07e-03±6.18e-02	0.14±2.61e-03±1.60e-02
0.80	0.90	0.42 ±7.92e-03±4.97e-02	0.11±2.59e-03±1.25e-02
0.90	1.0	0.31 ±6.17e-03±3.67e-02	7.70e-02±1.99e-03±8.69e-03
1.0	1.10	0.23 ±4.64e-03±2.72e-02	5.59e-02±1.47e-03±6.25e-03
1.10	1.20	0.17 ±3.50e-03±2.01e-02	3.95e-02±1.08e-03±4.43e-03
1.20	1.30	0.13 ±2.57e-03±1.47e-02	2.79e-02±7.97e-04±3.13e-03
1.30	1.40	9.06e-02 ±1.90e-03±1.07e-02	1.90e-02±5.92e-04±2.17e-03
1.40	1.50	6.50e-02 ±1.39e-03±7.99e-03	1.28e-02±4.43e-04±1.52e-03
1.50	1.60	4.56e-02 ±1.02e-03±6.11e-03	9.16e-03±3.37e-04±1.17e-03
1.60	1.70	3.22e-02 ±7.44e-04±4.98e-03	5.98e-03±2.52e-04±8.88e-04
1.70	1.80	2.25e-02 ±5.52e-04±3.44e-03	4.18e-03±2.02e-04±6.04e-04
1.80	1.90	1.61e-02 ±4.21e-04±2.42e-03	3.01e-03±1.56e-04±4.20e-04
1.90	2.0	1.10e-02 ±3.05e-04±1.63e-03	2.10e-03±1.21e-04±2.87e-04

TABLE XI. Invariant p_T spectra ($\frac{1}{2\pi}\frac{d^2N}{p_T dp_T dy}\pm$stat$\pm$sys (GeV/c)$^{-2}$) of primordial protons in 0-10%, 10-20% and 20-40% Au+Au collisions at $\sqrt{s_{NN}}$ = 39 GeV.

p_T^{low}	p_T^{high}	$\frac{1}{2\pi}\frac{d^2N}{p_T dy dp_T}$		
		0-10%	10-20%	20-40%
0.40	0.45	4.34 ±2.59e-02±0.92	2.96±2.51e-02±0.72	1.99±1.47e-02 ±0.46
0.45	0.50	4.0 ±2.56e-02±0.71	2.77±2.39e-02±0.54	1.87±1.39e-02 ±0.34
0.50	0.55	3.76 ±2.48e-02±0.59	2.66±2.26e-02±0.44	1.75±1.28e-02 ±0.28
0.55	0.60	3.56 ±2.38e-02±0.52	2.54±2.09e-02±0.38	1.62±1.17e-02 ±0.23
0.60	0.65	3.34 ±2.29e-02±0.48	2.41±1.92e-02±0.34	1.51±1.07e-02 ±0.20
0.65	0.70	3.13 ±2.17e-02±0.44	2.29±1.77e-02±0.31	1.38±9.84e-03 ±0.18
0.70	0.75	2.94 ±2.02e-02±0.40	2.15±1.60e-02±0.28	1.27±8.94e-03 ±0.16
0.75	0.80	2.68 ±1.90e-02±0.36	1.97±1.46e-02±0.26	1.17±8.11e-03 ±0.15
0.80	0.90	2.32 ±2.29e-02±0.31	1.70±1.74e-02±0.22	0.99±9.40e-03 ±0.12
0.90	1.0	1.93 ±1.93e-02±0.26	1.39±1.43e-02±0.17	0.79±7.49e-03 ±9.63e-02
1.0	1.10	1.58 ±1.56e-02±0.21	1.12±1.15e-02±0.14	0.62±5.91e-03 ±7.48e-02
1.10	1.20	1.28 ±1.25e-02±0.16	0.89±9.12e-03±0.11	0.48±4.70e-03 ±5.75e-02
1.20	1.30	1.01 ±9.75e-03±0.13	0.69±7.16e-03±8.29e-02	0.37±3.62e-03 ±4.38e-02
1.30	1.40	0.78 ±7.56e-03±9.91e-02	0.52±5.47e-03±6.36e-02	0.27±2.81e-03 ±3.33e-02
1.40	1.50	0.58 ±5.69e-03±7.72e-02	0.38±4.24e-03±4.94e-02	0.20±2.16e-03 ±2.57e-02
1.50	1.60	0.43 ±4.25e-03±6.20e-02	0.28±3.22e-03±3.96e-02	0.15±1.65e-03 ±2.06e-02
1.60	1.70	0.32 ±3.17e-03±5.23e-02	0.20±2.41e-03±3.39e-02	0.11±1.25e-03 ±1.75e-02
1.70	1.80	0.23 ±2.32e-03±3.74e-02	0.15±1.81e-03±2.46e-02	7.66e-02±9.43e-04 ±1.26e-02
1.80	1.90	0.16 ±1.71e-03±2.66e-02	0.11±1.34e-03±1.77e-02	5.55e-02±7.17e-04 ±9.09e-03
1.90	2.0	0.12 ±1.26e-03±1.88e-02	7.67e-02±9.82e-04±1.27e-02	3.99e-02±5.41e-04 ±6.52e-03

TABLE XII. Invariant p_T spectra ($\frac{1}{2\pi}\frac{d^2N}{p_T dp_T dy}\pm$stat$\pm$sys (GeV/c)$^{-2}$) of primordial protons in 40-60% and 60-80% Au+Au collisions at $\sqrt{s_{NN}}$ = 39 GeV.

p_T^{low}	p_T^{high}	$\frac{1}{2\pi}\frac{d^2N}{p_T dy dp_T}$	
		40-60%	60-80%
0.40	0.45	0.86 ±9.96e-03±0.21	0.34±3.87e-03±6.40e-02
0.45	0.50	0.82 ±9.29e-03±0.16	0.31±3.55e-03±4.61e-02
0.50	0.55	0.76 ±8.73e-03±0.13	0.28±3.20e-03±3.62e-02
0.55	0.60	0.68 ±8.04e-03±0.11	0.25±2.90e-03±2.92e-02
0.60	0.65	0.62 ±7.22e-03±9.55e-02	0.21±2.54e-03±2.43e-02
0.65	0.70	0.55 ±6.52e-03±8.19e-02	0.18±2.24e-03±2.04e-02
0.70	0.75	0.50 ±5.93e-03±6.99e-02	0.16±2.01e-03±1.75e-02
0.75	0.80	0.45 ±5.27e-03±5.97e-02	0.14±1.79e-03±1.51e-02
0.80	0.90	0.37 ±6.04e-03±4.77e-02	0.11±1.86e-03±1.21e-02
0.90	1.0	0.28 ±4.73e-03±3.49e-02	7.86e-02±1.43e-03±8.68e-03
1.0	1.10	0.21 ±3.58e-03±2.55e-02	5.52e-02±1.11e-03±6.20e-03
1.10	1.20	0.16 ±2.67e-03±1.90e-02	3.89e-02±8.50e-04±4.43e-03
1.20	1.30	0.12 ±2.02e-03±1.42e-02	2.75e-02±6.50e-04±3.16e-03
1.30	1.40	8.96e-02 ±1.48e-03±1.06e-02	1.91e-02±4.85e-04±2.25e-03
1.40	1.50	6.53e-02 ±1.10e-03±8.10e-03	1.32e-02±3.63e-04±1.65e-03
1.50	1.60	4.72e-02 ±7.93e-04±6.39e-03	9.04e-03±2.73e-04±1.24e-03
1.60	1.70	3.40e-02 ±5.88e-04±5.33e-03	6.28e-03±2.07e-04±1.01e-03
1.70	1.80	2.45e-02 ±4.27e-04±3.78e-03	4.40e-03±1.48e-04±6.96e-04
1.80	1.90	1.75e-02 ±3.11e-04±2.66e-03	2.97e-03±1.10e-04±4.72e-04
1.90	2.0	1.26e-02 ±2.37e-04±1.88e-03	2.04e-03±8.0e-5±3.20e-04

TABLE XIII. Invariant p_T spectra ($\frac{1}{2\pi}\frac{d^2N}{p_T dp_T dy}\pm$stat$\pm$sys (GeV/c)$^{-2}$) of primordial protons in 0-10%, 10-20% and 20-40% Au+Au collisions at $\sqrt{s_{NN}}$ = 54.4 GeV.

p_T^{low}	p_T^{high}	$\frac{1}{2\pi}\frac{d^2N}{p_T dy dp_T}$		
		0-10%	10-20%	20-40%
0.4	0.5	3.36±9.31e-02±0.94	2.32±8.0e-02±0.66	1.37±5.25e-02±0.38
0.5	0.6	3.10±8.74e-02±0.83	2.21±7.89e-02±0.59	1.30±4.53e-02±0.32
0.6	0.7	2.90±8.11e-02±0.70	2.10±6.63e-02±0.530	1.22±3.69e-02±0.28
0.7	0.8	2.62±7.04e-02±0.52	1.85±5.88e-02±0.42	1.06±3.15e-02±0.22
0.8	0.9	2.30±6.00e-02±0.39	1.61±4.97e-02±0.33	0.91±2.42e-02±0.16
0.9	1.0	1.85±4.95e-02±0.28	1.29±4.09e-02±0.25	0.72±1.96e-02±0.11
1.0	1.1	1.53±4.08e-02±0.33	0.97±3.35e-02±0.22	0.59±1.58e-02±7.97e-02
1.1	1.2	1.24±3.23e-02±0.25	0.78±2.67e-02±0.19	0.46±1.25e-02±4.63e-02
1.2	1.3	0.97±2.65e-02±0.20	0.61±2.02e-02±0.14	0.35±1.03e-02±4.19e-02
1.3	1.4	0.74±2.01e-02±0.15	0.48±1.59e-02±8.97e-02	0.26±7.63e-03±3.03e-02
1.4	1.5	0.56±1.54e-02±0.12	0.35±1.22e-02±7.93e-02	0.19±6.13e-03±2.73e-02
1.5	1.6	0.41±1.16e-02±9.16e-02	0.26±9.13e-03±5.96e-02	0.14±4.51e-03±1.69e-02
1.6	1.7	0.30±8.50e-03±7.0e-02	0.19±6.70e-03±4.40e-02	0.10±3.42e-03±1.27e-02
1.7	1.8	0.22±6.38e-03±5.31e-02	0.14±4.91e-03±3.28e-02	7.24e-02±2.62e-03±9.51e-03
1.8	1.9	0.16±4.52e-03±4.00e-02	9.93e-02±3.66e-03±2.42e-02	5.19e-02±1.92e-03±7.01e-03
1.9	2.0	0.11±3.31e-03±2.95e-02	7.16e-02±2.64e-03±1.77e-02	3.75e-02±1.41e-03±5.13e-03
2.0	2.1	7.79e-02±2.38e-03±2.14e-02	5.15e-02±1.89e-03±1.28e-02	2.69e-02±1.0e-03±3.69e-03
2.1	2.2	5.48e-02±1.70e-03±1.54e-02	3.74e-02±1.35e-03±9.28e-03	1.95e-02±7.52e-04±2.66e-03

TABLE XIV. Invariant p_T spectra ($\frac{1}{2\pi}\frac{d^2N}{p_T dp_T dy}\pm$stat$\pm$sys (GeV/c)$^{-2}$) of primordial protons in 40-60% and 60-80% Au+Au collisions at $\sqrt{s_{NN}}$ = 54.4 GeV.

p_T^{low}	p_T^{high}	$\frac{1}{2\pi}\frac{d^2N}{p_T dy dp_T}$	
		40-60%	60-80%
0.4	0.5	0.69±3.51e-02±0.17	0.24±1.81e-02±6.10e-02
0.5	0.6	0.61±3.21e-02±0.15	0.21±1.59e-02±4.63e-02
0.6	0.7	0.53±2.67e-02±0.12	0.16±1.20e-02±3.48e-02
0.7	0.8	0.42±2.06e-02±8.59e-02	0.12±9.72e-03±2.42e-02
0.8	0.9	0.34±1.60e-02±5.56e-02	9.19e-02±7.23e-03±1.52e-02
0.9	1.0	0.26±1.29e-02±3.67e-02	6.74e-02±5.15e-03±1.01e-02
1.0	1.1	0.20±9.98e-03±2.45e-02	5.06e-02±3.73e-03±5.61e-03
1.1	1.2	0.15±7.79e-03±1.73e-02	3.71e-02±2.86e-03±3.61e-03
1.2	1.3	0.11±5.53e-03±1.19e-02	2.68e-02±1.96e-03±2.43e-03
1.3	1.4	8.46e-02±4.20e-03±8.64e-03	1.92e-02±1.39e-03±1.89e-03
1.4	1.5	6.19e-02±3.12e-03±6.45e-03	1.36e-02±9.86e-04±1.38e-03
1.5	1.6	4.49e-02±2.33e-03±4.80e-03	9.59e-03±6.88e-04±9.99e-04
1.6	1.7	3.24e-02±1.63e-03±3.53e-03	6.58e-03±4.75e-04±7.10e-04
1.7	1.8	2.36e-02±1.19e-03±2.57e-03	4.60e-03±3.43e-04±4.91e-04
1.8	1.9	1.71e-02±7.93e-04±1.81e-03	3.09e-03±2.73e-04±3.42e-04
1.9	2.0	1.22e-02±5.83e-04±1.28e-03	2.19e-03±1.69e-04±2.35e-04
2.0	2.1	8.82e-03±3.91e-04±8.88e-04	1.45e-03±1.14e-04±1.49e-04
2.1	2.2	6.22e-03±2.51e-04±6.22e-04	9.98e-04±9.60e-05±1.02e-04

TABLE XV. Invariant p_T spectra ($\frac{1}{2\pi}\frac{d^2N}{p_T dp_T dy}\pm$stat$\pm$sys (GeV/c)$^{-2}$) of primordial protons in 0-10%, 10-20% and 20-40% Au+Au collisions at $\sqrt{s_{NN}}$ = 62.4 GeV.

p_T^{low}	p_T^{high}	$\frac{1}{2\pi}\frac{d^2N}{p_T dy dp_T}$		
		0-10%	10-20%	20-40%
0.5	0.6	2.89±0.24±0.50	2.24±0.20±0.37	1.51±0.11±0.23
0.6	0.7	2.57±0.18±0.45	2.12±0.16±0.34	1.26±8.03e-02±0.20
0.7	0.8	2.60±0.16±0.42	1.86±0.13±0.29	1.11±6.52e-02±0.17
0.8	0.9	2.27±0.13±0.35	1.58±0.10±0.25	0.93±5.29e-02±0.14
0.9	1.0	2.04±0.11±0.30	1.46±9.22e-02±0.21	0.76±4.44e-02±0.11
1.0	1.2	1.74±6.44e-02±0.23	1.15±5.16e-02±0.15	0.65±2.66e-02±8.50e-02
1.2	1.4	1.08±4.20e-02±0.14	0.74±3.30e-02±9.24e-02	0.40±1.72e-02±5.04e-02
1.4	1.6	0.62±2.66e-02±7.64e-02	0.41±2.12e-02±5.13e-02	0.21±1.05e-02±2.63e-02
1.6	1.8	0.35±1.75e-02±4.18e-02	0.20±1.34e-02±2.53e-02	0.11±6.75e-03±1.37e-02
1.8	2.0	0.18±1.16e-02±2.19e-02	0.13±9.31e-03±1.51e-02	6.53e-02±4.47e-03±7.80e-03
2.0	2.5	6.36e-02±3.59e-03±7.10e-03	4.24e-02±3.0e-03±4.84e-03	2.21e-02±1.45e-03±2.47e-03
2.5	3.0	1.21e-02±1.15e-03±2.13e-03	7.88e-03±8.93e-04±1.42e-03	5.09e-03±1.39e-04±8.67e-04

TABLE XVI. Invariant p_T spectra ($\frac{1}{2\pi}\frac{d^2N}{p_T dp_T dy}\pm$stat$\pm$sys (GeV/c)$^{-2}$) of primordial protons in 40-80% Au+Au collisions at $\sqrt{s_{\mathrm{NN}}}$ = 62.4 GeV.

p_T^{low}	p_T^{high}	$\frac{1}{2\pi}\frac{d^2N}{p_T dy dp_T}$
		40-80%
0.5	0.6	0.34±3.34e-02±5.50e-02
0.6	0.7	0.38±2.81e-02±5.28e-02
0.7	0.8	0.27±2.20e-02±4.03e-02
0.8	0.9	0.26±1.98e-02±3.52e-02
0.9	1.0	0.18±1.47e-02±2.52e-02
1.0	1.2	0.15±8.62e-03±1.88e-02
1.2	1.4	7.83e-02±5.26e-03±1.01e-02
1.4	1.6	3.85e-02±3.10e-03±5.11e-03
1.6	1.8	2.04e-02±2.02e-03±2.65e-03
1.8	2.0	1.03e-02±1.23e-03±1.31e-03
2.0	2.5	4.35e-03±4.32e-04±4.71e-04
2.5	3.0	9.36e-04±9.60e-5±1.55e-04

TABLE XVII. Invariant p_T spectra ($\frac{1}{2\pi}\frac{d^2N}{p_T dp_T dy}\pm$stat$\pm$sys (GeV/c)$^{-2}$) of primordial protons in 0-12%, 10-20% and 20-40% Au+Au collisions at $\sqrt{s_{\mathrm{NN}}}$ = 200 GeV.

p_T^{low}	p_T^{high}	$\frac{1}{2\pi}\frac{d^2N}{p_T dy dp_T}$	p_T^{low}	p_T^{high}	$\frac{1}{2\pi}\frac{d^2N}{p_T dy dp_T}$	p_T^{low}	p_T^{high}	$\frac{1}{2\pi}\frac{d^2N}{p_T dy dp_T}$
		0-10%			10-20%			20-40%
0.50	0.60	1.88 ± 1.12	0.50	0.60	2.10 ±0.86	0.50	0.60	1.31 ±0.45
0.60	0.70	2.28 ± 0.94	0.60	0.70	2.18 ±0.73	0.60	0.70	1.44 ±0.38
0.70	0.80	2.58 ± 0.77	0.70	0.80	2.11 ±0.65	0.70	0.80	1.33 ±0.33
0.80	0.90	2.53 ± 0.67	0.80	0.90	1.92 ±0.59	0.80	0.90	1.15 ±0.29
0.90	1.0	2.29 ± 0.59	0.90	1.0	1.73 ±0.53	0.90	1.0	1.02 ±0.26
1.0	1.10	2.13 ± 0.50	1.0	1.10	1.63 ±0.41	1.0	1.10	0.95 ±0.21
1.10	1.20	1.66 ± 0.44	1.10	1.20	1.21 ±0.32	1.10	1.20	0.68 ±0.17
1.20	1.40	1.13 ± 0.31	1.20	1.40	0.82 ±0.23	1.20	1.40	0.43 ±0.12
1.40	1.60	0.69 ± 0.20	1.40	1.60	0.51 ±0.14	1.40	1.60	0.26 ±6.87e-02
1.60	1.80	0.40 ± 0.12	1.60	1.80	0.29 ±8.28e-02	1.60	1.80	0.15 ±4.09e-02
1.80	2.0	0.24 ± 6.93e-02	1.80	2.0	0.17 ±4.86e-02	1.80	2.0	9.17e-02 ±2.48e-02
2.0	2.20	0.15 ± 4.87e-02	2.0	2.20	0.11 ±3.31e-02	2.0	2.20	5.82e-02 ±1.69e-02
2.20	2.50	7.68e-02 ± 2.41e-02	2.20	2.50	5.48e-02 ±1.72e-02	2.20	2.50	2.89e-02 ±8.62e-03
2.50	2.75	2.59e-02 ± 1.07e-02	2.50	3.0	1.77e-02 ±5.49e-03	2.50	3.0	9.84e-03 ±2.91e-03
2.75	3.0	1.23e-02± 5.06e-03	3.0	3.25	4.70e-03 ±2.01e-03	3.0	3.25	2.45e-03 ±1.03e-03
3.0	3.25	5.92e-03± 2.67e-03	3.25	3.50	2.41e-03 ±1.08e-03	3.25	3.50	1.24e-03 ±5.44e-04
3.25	3.50	3.03e-03± 1.36e-03	3.50	3.75	1.29e-03 ±5.62e-04	3.50	3.75	6.92e-04 ±2.98e-04
3.50	3.75	1.52e-03± 7.45e-04	3.75	4.0	7.37e-04 ±2.89e-04	3.75	4.0	4.05e-04 ±1.55e-04
3.75	4.0	8.58e-04± 3.75e-04	4.0	4.5	3.39e-04 ±1.17e-04	4.0	4.5	1.96e-04 ±6.56e-05
4.0	4.50	4.20e-04± 1.39e-04	4.50	5.0	1.14e-04 ±4.28e-05	4.5	5.0	6.96e-05 ±2.53e-05
4.50	5.0	1.55e-04± 4.63e-05	5.0	5.5	4.93e-05 ±1.65e-05	5.0	5.5	3.10e-05 ±1.01e-05
5.0	5.50	5.69e-05± 1.66e-05	5.50	6.0	2.25e-05 ±8.85e-06	5.5	6.0	9.42e-06 ±3.76e-06
5.50	6.0	2.79e-05± 7.07e-06	6.0	7.0	7.91e-06 ±2.82e-06	6.0	7.0	3.92e-06 ±1.36e-06
6.0	7.0	9.04e-06± 2.40e-06	7.0	8.0	1.94e-06 ±8.42e-07	7.0	8.0	1.47e-06 ±5.03e-07
7.0	8.0	2.37e-06± 6.69e-07	8.0	10.0	5.78e-07 ±2.48e-07	8.0	10.0	4.02e-07 ±1.45e-07
8.0	10.0	6.94e-07± 1.88e-07						
10.0	12.0	1.54e-07 ± 7.87e-08						

TABLE XVIII. Invariant p_T spectra ($\frac{1}{2\pi}\frac{d^2N}{p_T dp_T dy}\pm$stat$\pm$sys (GeV/c)$^{-2}$) of primordial protons in 40-60% and 60-80% Au+Au collisions at $\sqrt{s_{NN}}$ = 200 GeV.

p_T^{low}	p_T^{high}	$\frac{1}{2\pi}\frac{d^2N}{p_T dy dp_T}$	p_T^{low}	p_T^{high}	$\frac{1}{2\pi}\frac{d^2N}{p_T dy dp_T}$
		40-60%			60-80%
0.50	0.60	0.81 ±0.21	0.50	0.60	0.30 ±8.59e-02
0.60	0.70	0.66 ±0.18	0.60	0.70	0.24 ±6.84e-02
0.70	0.80	0.59 ±0.15	0.70	0.80	0.20 ±5.34e-02
0.80	0.90	0.52 ±0.13	0.80	0.90	0.17 ±4.32e-02
0.90	1.0	0.45 ±0.11	0.90	1.0	0.14 ±3.51e-02
1.0	1.10	0.43 ±8.66e-02	1.0	1.10	0.13 ±2.91e-02
1.10	1.20	0.31 ±6.45e-02	1.10	1.20	8.67e-02 ±1.87e-02
1.20	1.40	0.18 ±4.54e-02	1.20	1.40	5.11e-02 ±1.15e-02
1.40	1.60	0.10 ±2.61e-02	1.40	1.60	3.03e-02 ±9.83e-02
1.60	1.80	6.04e-02 ±1.49e-02	1.60	1.80	1.41e-02 ±5.53e-02
1.80	2.0	3.57e-02 ±8.71e-03	1.80	2.0	7.47e-03 ±2.94e-02
2.0	2.20	2.06e-02 ±5.95e-03	2.0	2.20	3.81e-03 ±1.65e-02
2.20	2.50	9.38e-03 ±2.84e-03	2.20	2.50	1.83e-03 ±9.21e-04
2.50	3.0	3.79e-03 ±1.07e-03	2.50	3.0	6.87e-04 ±3.29e-04
3.0	3.25	9.18e-04±4.28e-04	3.0	3.25	2.12e-04±1.08e-04
3.25	3.50	4.99e-04±2.37e-04	3.25	3.50	1.14e-04±5.99e-05
3.50	3.75	2.53e-04±1.28e-04	3.50	3.75	6.52e-05±3.25e-05
3.75	4.0	1.65e-04±7.03e-05	3.75	4.0	4.10e-05 ±1.70e-05
4.0	4.50	9.15e-05±2.91e-05	4.0	4.50	2.39e-05±8.05e-06
4.50	5.0	3.39e-05±1.10e-05	4.50	5.0	8.56e-06±3.21e-06
5.0	5.50	1.38e-05±4.54e-06	5.0	5.50	4.39e-06±1.53e-06
5.50	6.0	5.21e-06±2.29e-06	5.50	6.0	1.46e-06±7.95e-07
6.0	7.0	1.83e-06±8.04e-07	6.0	7.0	6.08e-07±3.13e-07
7.0	8.0	7.16e-07±3.08e-07	7.0	8.0	2.45e-07±1.35e-07
8.0	10.0	1.30e-07 ±7.03e-08			

Appendix B: Invariant transverse momentum (p_T) spectra of primordial antiprotons in Au+Au collisions at $\sqrt{s_{\mathrm{NN}}}$ = 7.7 - 200 GeV.

TABLE XIX. Invariant p_T spectra ($\frac{1}{2\pi}\frac{d^2N}{p_T dp_T dy}\pm$stat$\pm$sys (GeV/c)$^{-2}$) of primordial antiprotons in 0-10%, 10-20% and 20-40% Au+Au collisions at $\sqrt{s_{\mathrm{NN}}}$ = 7.7 GeV.

p_T^{low}	p_T^{high}	$\frac{1}{2\pi}\frac{d^2N}{p_T dy dp_T}$		
		0-10%	10-20%	20-40%
0.40	0.45	5.19e-02 ±8.47e-03 ±1.43e-02	5.70e-02 ±3.82e-03 ±1.49e-02	3.42e-02 ±4.36e-03 ±8.15e-03
0.45	0.50	4.85e-02 ±7.71e-03 ±1.16e-02	4.95e-02 ±3.41e-03 ±1.18e-02	2.85e-02 ±3.84e-03 ±6.22e-03
0.50	0.55	4.34e-02 ±7.07e-03 ±9.95e-03	4.40e-02 ±3.10e-03 ±9.76e-03	2.73e-02 ±3.53e-03 ±5.30e-03
0.55	0.60	4.35e-02 ±6.62e-03 ±9.03e-03	3.52e-02 ±2.78e-03 ±7.98e-03	2.54e-02 ±3.26e-03 ±4.61e-03
0.60	0.65	3.94e-02 ±6.10e-03 ±8.04e-03	3.55e-02 ±2.63e-03 ±6.97e-03	2.18e-02 ±2.92e-03 ±3.96e-03
0.65	0.70	3.51e-02 ±5.61e-03 ±7.17e-03	3.36e-02 ±2.44e-03 ±6.10e-03	2.03e-02 ±2.69e-03 ±3.57e-03
0.70	0.75	3.14e-02 ±5.17e-03 ±6.41e-03	2.57e-02 ±2.17e-03 ±4.97e-03	1.71e-02 ±2.41e-03 ±3.09e-03
0.75	0.80	2.91e-02 ±4.80e-03 ±5.83e-03	2.33e-02 ±2.00e-03 ±4.39e-03	1.47e-02 ±2.19e-03 ±2.70e-03
0.80	0.90	2.38e-02 ±5.03e-03 ±4.90e-03	1.56e-02 ±1.68e-03 ±3.48e-03	1.16e-02 ±2.30e-03 ±2.21e-03
0.90	1.0	2.21e-02 ±3.26e-03 ±4.13e-03	1.37e-02 ±1.33e-03 ±2.89e-03	9.33e-03 ±1.41e-03 ±1.71e-03
1.0	1.10	1.60e-02 ±2.69e-03 ±3.13e-03	1.08e-02 ±1.11e-03 ±2.31e-03	6.77e-03 ±1.13e-03 ±1.26e-03
1.10	1.20	1.28e-02 ±2.24e-03 ±2.42e-03	7.78e-03 ±8.94e-04 ±1.77e-03	4.98e-03 ±8.97e-04 ±9.20e-04
1.20	1.30	9.87e-03 ±1.86e-03 ±1.85e-03	5.19e-03 ±7.09e-04 ±1.29e-03	3.74e-03 ±7.39e-04 ±6.75e-04

TABLE XX. Invariant p_T spectra ($\frac{1}{2\pi}\frac{d^2N}{p_T dp_T dy}\pm$stat$\pm$sys (GeV/c)$^{-2}$) of primordial antiprotons in 40-60% and 60-80% Au+Au collisions at $\sqrt{s_{\mathrm{NN}}}$ = 7.7 GeV.

p_T^{low}	p_T^{high}	$\frac{1}{2\pi}\frac{d^2N}{p_T dy dp_T}$	p_T^{low}	p_T^{high}	$\frac{1}{2\pi}\frac{d^2N}{p_T dy dp_T}$
		40-60%			60-80%
0.40	0.45	2.27e-02 ±3.33e-03 ±4.52e-03	0.40	0.45	9.49e-03 ±2.03e-03 ±1.50e-03
0.45	0.50	2.13e-02 ±2.98e-03 ±3.53e-03	0.45	0.50	8.56e-03 ±1.87e-03 ±1.14e-03
0.50	0.55	1.75e-02 ±2.61e-03 ±2.81e-03	0.50	0.55	6.36e-03 ±1.60e-03 ±8.63e-04
0.55	0.60	1.47e-02 ±2.30e-03 ±2.33e-03	0.55	0.60	6.03e-03 ±1.51e-03 ±8.24e-04
0.60	0.65	1.22e-02 ±2.05e-03 ±1.97e-03	0.60	0.65	5.02e-03 ±1.30e-03 ±6.24e-04
0.65	0.70	9.87e-03 ±1.80e-03 ±1.63e-03	0.65	0.70	3.68e-03 ±1.12e-03 ±5.06e-04
0.70	0.75	8.57e-03 ±1.64e-03 ±1.40e-03	0.70	0.80	2.85e-03 ±1.21e-03 ±4.08e-04
0.75	0.80	7.74e-03 ±1.49e-03 ±1.23e-03			
0.80	0.90	5.25e-03 ±1.09e-03 ±9.20e-04			
0.90	1.0	3.38e-03 ±8.33e-04 ±6.32e-04			
1.0	1.10	3.0e-03 ±7.17e-04 ±4.86e-04			

TABLE XXI. Invariant p_T spectra ($\frac{1}{2\pi}\frac{d^2N}{p_T dp_T dy}\pm$stat$\pm$sys (GeV/c)$^{-2}$) of primordial antiprotons in 0-10%, 10-20% and 20-40% Au+Au collisions at $\sqrt{s_{NN}}$ = 11.5 GeV.

p_T^{low}	p_T^{high}	$\frac{1}{2\pi}\frac{d^2N}{p_T dy dp_T}$		
		0-10%	10-20%	20-40%
0.40	0.45	0.20±1.10e-02 ±5.46e-02	0.14 ±4.86e-03 ±3.85e-02	0.11 ±5.54e-03 ±2.59e-02
0.45	0.50	0.19±1.01e-02 ±4.43e-02	0.14 ±4.53e-03 ±3.18e-02	0.10 ±5.05e-03 ±2.07e-02
0.50	0.55	0.17±9.26e-03 ±3.72e-02	0.13 ±4.20e-03 ±2.76e-02	8.94e-02 ±4.59e-03 ±1.74e-02
0.55	0.60	0.17±8.72e-03 ±3.31e-02	0.12 ±3.93e-03 ±2.47e-02	8.30e-02 ±4.19e-03 ±1.55e-02
0.60	0.65	0.17±8.25e-03 ±3.01e-02	0.12 ±3.66e-03 ±2.22e-02	8.27e-02 ±3.93e-03 ±1.44e-02
0.65	0.70	0.15±7.64e-03 ±2.69e-02	0.11 ±3.37e-03 ±1.98e-02	7.25e-02 ±3.57e-03 ±1.27e-02
0.70	0.75	0.14±7.05e-03 ±2.42e-02	9.82e-02 ±3.10e-03 ±1.77e-02	6.16e-02 ±3.22e-03 ±1.10e-02
0.75	0.80	0.12±6.45e-03 ±2.14e-02	8.79e-02 ±2.85e-03 ±1.56e-02	5.76e-02 ±2.97e-03 ±9.91e-03
0.80	0.90	9.73e-02±5.24e-03 ±1.78e-02	7.63e-02 ±2.56e-03 ±1.32e-02	4.26e-02 ±2.36e-03 ±7.80e-03
0.90	1.0	8.17e-02±4.45e-03 ±1.46e-02	5.77e-02 ±2.11e-03 ±1.01e-02	3.44e-02 ±1.95e-03 ±6.01e-03
1.0	1.10	6.38e-02±3.69e-03 ±1.14e-02	4.66e-02 ±1.73e-03 ±7.88e-03	2.51e-02 ±1.58e-03 ±4.40e-03
1.10	1.20	4.90e-02±3.03e-03 ±8.71e-03	3.42e-02 ±1.37e-03 ±5.87e-03	1.81e-02 ±1.27e-03 ±3.17e-03
1.20	1.30	3.90e-02±2.50e-03 ±6.63e-03	2.49e-02 ±1.09e-03 ±4.33e-03	1.38e-02 ±1.02e-03 ±2.31e-03
1.30	1.40	2.68e-02±1.99e-03 ±4.74e-03	1.55e-02 ±8.27e-04 ±2.98e-03	8.41e-03 ±7.91e-04 ±1.55e-03
1.40	1.50	1.94e-02±1.59e-03 ±3.49e-03	1.22e-02 ±6.65e-04 ±2.28e-03	6.03e-03 ±6.14e-04 ±1.12e-03
1.50	1.60	1.30e-02±1.26e-03 ±2.58e-03	8.03e-03 ±5.14e-04 ±1.68e-03	4.15e-03 ±4.96e-04 ±8.27e-04
1.60	1.70	7.49e-03±9.44e-04 ±1.87e-03	5.26e-03 ±3.96e-04 ±1.29e-03	2.67e-03 ±3.82e-04 ±6.26e-04
1.70	1.80	5.49e-03±7.65e-04 ±1.30e-03	2.87e-03 ±2.96e-04 ±7.89e-04	1.53e-03 ±2.91e-04 ±3.93e-04
1.80	1.90	3.97e-03±6.23e-04 ±9.03e-04	1.80e-03 ±2.20e-04 ±5.13e-04	
1.90	2.0	2.30e-03±4.66e-04 ±5.78e-04	1.13e-03 ±1.66e-04 ±3.25e-04	

TABLE XXII. Invariant p_T spectra ($\frac{1}{2\pi}\frac{d^2N}{p_T dp_T dy}\pm$stat$\pm$sys (GeV/c)$^{-2}$) of primordial antiprotons in 40-60% and 60-80% Au+Au collisions at $\sqrt{s_{NN}}$ = 11.5 GeV.

p_T^{low}	p_T^{high}	$\frac{1}{2\pi}\frac{d^2N}{p_T dy dp_T}$	p_T^{low}	p_T^{high}	$\frac{1}{2\pi}\frac{d^2N}{p_T dy dp_T}$
		40-60%			60-80%
0.40	0.45	5.25e-02 ±4.19e-03 ±1.45e-02	0.40	0.45	2.65e-02 ±2.84e-03 ±5.70e-03
0.45	0.50	4.61e-02 ±3.75e-03 ±1.12e-02	0.45	0.50	2.26e-02 ±2.48e-03 ±4.29e-03
0.50	0.55	4.33e-02 ±3.41e-03 ±9.58e-03	0.50	0.55	2.02e-02 ±2.26e-03 ±3.57e-03
0.55	0.60	3.94e-02 ±3.08e-03 ±8.29e-03	0.55	0.60	1.66e-02 ±1.99e-03 ±2.97e-03
0.60	0.65	3.35e-02 ±2.76e-03 ±7.15e-03	0.60	0.65	1.36e-02 ±1.74e-03 ±2.49e-03
0.65	0.70	2.85e-02 ±2.47e-03 ±6.15e-03	0.65	0.70	1.18e-02 ±1.55e-03 ±2.12e-03
0.70	0.80	2.21e-02 ±2.00e-03 ±4.87e-03	0.70	0.80	8.65e-03 ±1.19e-03 ±1.60e-03
0.80	0.90	1.63e-02 ±1.58e-03 ±3.50e-03	0.80	0.90	5.31e-03 ±8.90e-04 ±1.04e-03
0.90	1.00	1.07e-02 ±1.24e-03 ±2.42e-03	0.90	1.00	3.24e-03 ±6.71e-04 ±6.48e-04
1.00	1.10	8.60e-03 ±9.87e-04 ±1.75e-03	1.00	1.10	2.34e-03 ±5.38e-04 ±4.20e-04
1.10	1.20	6.05e-03 ±7.69e-04 ±1.21e-03	1.10	1.20	2.24e-03 ±4.25e-04 ±3.22e-04
1.20	1.30	3.60e-03 ±5.78e-04 ±7.78e-04			
1.30	1.40	2.45e-03 ±4.48e-04 ±5.31e-04			
1.40	1.50	1.17e-03 ±3.20e-04 ±3.34e-04			
1.50	1.60	1.10e-03 ±2.61e-04 ±2.71e-04			

TABLE XXIII. Invariant p_T spectra ($\frac{1}{2\pi}\frac{d^2N}{p_T dp_T dy}\pm$stat$\pm$sys (GeV/c)$^{-2}$) of primordial antiprotons in 0-10%, 10-20% and 20-40% Au+Au collisions at $\sqrt{s_{NN}}$ = 14.5 GeV.

p_T^{low}	p_T^{high}	$\frac{1}{2\pi}\frac{d^2N}{p_T dy dp_T}$		
		0-10%	10-20%	20-40%
0.50	0.55	0.35±8.85e-03 ±8.52e-02	0.27 ±5.28e-03 ±6.23e-02	0.20 ±5.16e-03 ±3.76e-02
0.55	0.60	0.32±8.27e-03 ±7.39e-02	0.25 ±5.06e-03 ±5.48e-02	0.17 ±4.82e-03 ±3.35e-02
0.60	0.65	0.30±7.83e-03 ±6.63e-02	0.22 ±4.89e-03 ±4.81e-02	0.16 ±4.43e-03 ±3.01e-02
0.65	0.70	0.28±7.37e-03 ±5.89e-02	0.20 ±4.64e-03 ±4.26e-02	0.14 ±4.12e-03 ±2.70e-02
0.70	0.75	0.26±6.97e-03 ±5.32e-02	0.18 ±4.36e-03 ±3.83e-02	0.13 ±3.79e-03 ±2.44e-02
0.75	0.80	0.24±6.51e-03 ±4.83e-02	0.17 ±4.08e-03 ±3.50e-02	0.11 ±3.46e-03 ±2.17e-02
0.80	0.85	0.21±6.17e-03 ±4.28e-02	0.15 ±3.85e-03 ±3.07e-02	0.10 ±3.27e-03 ±1.94e-02
0.85	0.90	0.19±5.82e-03 ±3.81e-02	0.13 ±3.58e-03 ±2.69e-02	8.72e-02 ±2.96e-03 ±1.67e-02
0.90	0.95	0.17±5.59e-03 ±3.41e-02	0.12 ±3.36e-03 ±2.45e-02	7.61e-02 ±2.85e-03 ±1.46e-02
0.95	1.00	0.15±5.44e-03 ±3.03e-02	0.11 ±3.18e-03 ±2.21e-02	6.62e-02 ±2.67e-03 ±1.29e-02
1.00	1.10	0.13±4.88e-03 ±2.57e-02	8.74e-02 ±3.00e-03 ±1.79e-02	5.46e-02 ±2.10e-03 ±1.03e-02
1.10	1.20	0.10±4.03e-03 ±2.02e-02	6.57e-02 ±2.38e-03 ±1.35e-02	4.01e-02 ±1.67e-03 ±7.52e-03
1.20	1.30	7.84e-02±3.27e-03 ±1.52e-02	5.11e-02 ±1.82e-03 ±1.01e-02	2.96e-02 ±1.32e-03 ±5.45e-03
1.30	1.40	5.34e-02±2.56e-03 ±1.06e-02	3.80e-02 ±1.39e-03 ±7.35e-03	2.21e-02 ±1.05e-03 ±3.95e-03
1.40	1.50	3.68e-02±2.01e-03 ±7.41e-03	2.63e-02 ±1.04e-03 ±5.05e-03	1.54e-02 ±8.22e-04 ±2.73e-03
1.50	1.60	2.81e-02±1.62e-03 ±5.38e-03	1.99e-02 ±7.92e-04 ±3.63e-03	1.10e-02 ±6.52e-04 ±1.90e-03
1.60	1.70	1.90e-02±1.27e-03 ±3.64e-03	1.41e-02 ±5.99e-04 ±2.49e-03	7.57e-03 ±5.21e-04 ±1.29e-03
1.70	1.80	1.31e-02±1.00e-03 ±2.47e-03	8.72e-04 ±4.49e-04 ±1.58e-03	5.83e-03 ±4.41e-04 ±9.34e-04
1.80	1.90	8.17e-03±7.74e-04 ±1.59e-03	7.61e-04 ±3.69e-04 ±1.22e-03	4.43e-03 ±3.73e-04 ±6.75e-04
1.90	2.00	5.10e-03±5.99e-04 ±1.02e-03	5.40e-04 ±2.93e-04 ±8.40e-04	2.77e-03 ±2.97e-04 ±4.25e-04

TABLE XXIV. Invariant p_T spectra ($\frac{1}{2\pi}\frac{d^2N}{p_T dp_T dy}\pm$stat$\pm$sys (GeV/c)$^{-2}$) of primordial antiprotons in 40-60% and 60-80% Au+Au collisions at $\sqrt{s_{NN}}$ = 14.5 GeV.

p_T^{low}	p_T^{high}	$\frac{1}{2\pi}\frac{d^2N}{p_T dy dp_T}$	p_T^{low}	p_T^{high}	$\frac{1}{2\pi}\frac{d^2N}{p_T dy dp_T}$
		40-60%			60-80%
0.50	0.55	9.08e-02 ±3.93e-03 ±1.72e-02	0.50	0.55	4.36e-02 ±2.62e-03 ±6.76e-03
0.55	0.60	8.36e-02 ±3.50e-03 ±1.54e-02	0.55	0.60	3.70e-02 ±2.33e-03 ±5.78e-03
0.60	0.65	7.31e-02 ±3.15e-03 ±1.34e-02	0.60	0.65	3.31e-02 ±2.02e-03 ±5.10e-03
0.65	0.70	6.19e-02 ±2.85e-03 ±1.15e-02	0.65	0.70	2.74e-02 ±1.86e-03 ±4.25e-03
0.70	0.75	5.86e-02 ±2.58e-03 ±1.05e-02	0.70	0.75	2.42e-02 ±1.57e-03 ±3.66e-03
0.75	0.80	5.22e-02 ±2.36e-03 ±9.16e-03	0.75	0.80	2.06e-02 ±1.41e-03 ±3.08e-03
0.80	0.85	4.46e-02 ±2.14e-03 ±7.83e-03	0.80	0.85	1.75e-02 ±1.28e-03 ±2.57e-03
0.85	0.90	3.66e-02 ±1.97e-03 ±6.49e-03	0.85	0.90	1.47e-02 ±1.18e-03 ±2.12e-03
0.90	0.95	3.17e-02 ±1.77e-03 ±5.57e-03	0.90	0.95	1.25e-02 ±1.02e-03 ±1.76e-03
0.95	1.00	2.68e-02 ±1.53e-03 ±4.69e-03	0.95	1.00	1.02e-02 ±9.70e-04 ±1.43e-03
1.00	1.10	1.85e-02 ±1.19e-03 ±3.39e-03			
1.10	1.20	1.33e-02 ±9.24e-04 ±2.39e-03			
1.20	1.30	9.62e-03 ±7.14e-04 ±1.69e-03			
1.30	1.40	6.12e-03 ±5.37e-04 ±1.10e-03			
1.40	1.50	3.72e-03 ±4.04e-04 ±6.90e-04			
1.50	1.60	2.26e-03 ±3.06e-04 ±4.34e-04			

TABLE XXV. Invariant p_T spectra ($\frac{1}{2\pi}\frac{d^2N}{p_T dp_T dy}$±stat±sys $(GeV/c)^{-2}$) of primordial antiprotons in 0-10%, 10-20% and 20-40% Au+Au collisions at $\sqrt{s_{NN}}$ = 19.6 GeV.

p_T^{low} p_T^{high}	$\frac{1}{2\pi}\frac{d^2N}{p_T dy dp_T}$		
	0-10%	10-20%	20-40%
0.40 0.45	0.58±1.24e-02 ±0.15	0.42 ±7.56e-03 ±0.11	0.30 ±6.63e-03 ±6.66e-02
0.45 0.50	0.55±1.17e-02 ±0.12	0.40 ±7.32e-03 ±8.58e-02	0.29 ±6.15e-03 ±5.36e-02
0.50 0.55	0.52±1.11e-02 ±0.10	0.39 ±6.94e-03 ±7.40e-02	0.27 ±5.79e-03 ±4.62e-02
0.55 0.60	0.49±1.05e-02 ±9.14e-02	0.37 ±6.63e-03 ±6.57e-02	0.26 ±7.02e-03 ±6.31e-02
0.60 0.65	0.46±9.90e-03 ±8.09e-02	0.34 ±6.30e-03 ±5.93e-02	0.24 ±6.29e-03 ±5.49e-02
0.65 0.70	0.43±9.33e-03 ±7.29e-02	0.32 ±5.96e-03 ±5.34e-02	0.22 ±4.59e-03 ±3.38e-02
0.70 0.75	0.41±8.68e-03 ±6.63e-02	0.30 ±5.55e-03 ±4.87e-02	0.20 ±4.22e-03 ±3.02e-02
0.75 0.80	0.38±8.13e-03 ±6.05e-02	0.28 ±5.09e-03 ±4.40e-02	0.18 ±3.87e-03 ±2.69e-02
0.80 0.90	0.31±8.12e-03 ±5.17e-02	0.23 ±5.77e-03 ±3.68e-02	0.15 ±3.77e-03 ±2.21e-02
0.90 1.00	0.26±6.82e-03 ±4.26e-02	0.18 ±4.76e-03 ±2.89e-02	0.11 ±3.05e-03 ±1.69e-02
1.00 1.10	0.21±5.59e-03 ±3.39e-02	0.15 ±3.83e-03 ±2.27e-02	8.53e-02 ±2.42e-03 ±1.27e-02
1.10 1.20	0.17±4.51e-03 ±2.64e-02	0.12 ±2.91e-03 ±1.75e-02	6.49e-02 ±1.91e-03 ±9.52e-03
1.20 1.30	0.13±3.63e-03 ±2.04e-02	8.75e-02 ±2.56e-03 ±1.32e-02	4.93e-02 ±1.50e-03 ±7.09e-03
1.30 1.40	9.55e-02±2.85e-03 ±1.50e-02	6.50e-02 ±1.71e-03 ±9.85e-03	3.52e-02 ±1.16e-03 ±5.15e-03
1.40 1.50	6.86e-02±2.20e-03 ±1.12e-02	4.51e-02 ±1.26e-03 ±7.22e-03	2.48e-02 ±8.89e-04 ±3.79e-03
1.50 1.60	4.80e-02±1.72e-03 ±8.50e-03	3.14e-02 ±9.41e-04 ±5.50e-03	1.76e-02 ±6.96e-04 ±2.91e-03
1.60 1.70	3.68e-02±1.37e-03 ±7.17e-03	2.30e-02 ±7.02e-04 ±4.56e-03	1.19e-02 ±5.33e-04 ±2.30e-03
1.70 1.80	2.59e-02±1.07e-03 ±4.96e-03	1.64e-02 ±5.27e-04 ±3.17e-03	8.57e-03 ±4.20e-04 ±1.62e-03
1.80 1.90	1.74e-02±8.39e-04 ±3.32e-03	1.09e-02 ±3.88e-04 ±2.12e-03	5.45e-03 ±3.25e-04 ±1.05e-03
1.90 2.00	1.17e-02±6.57e-04 ±2.23e-03	7.46e-03 ±2.99e-04 ±1.44e-03	3.92e-03 ±2.59e-04 ±7.29e-04

TABLE XXVI. Invariant p_T spectra ($\frac{1}{2\pi}\frac{d^2N}{p_T dp_T dy}$±stat±sys $(GeV/c)^{-2}$) of primordial antiprotons in 40-60% and 60-80% Au+Au collisions at $\sqrt{s_{NN}}$ = 19.6 GeV.

p_T^{low} p_T^{high}	$\frac{1}{2\pi}\frac{d^2N}{p_T dy dp_T}$	p_T^{low} p_T^{high}	$\frac{1}{2\pi}\frac{d^2N}{p_T dy dp_T}$
	40-60%		60-80%
0.40 0.45	0.19 ±5.11e-03 ±3.49e-02	0.40 0.45	8.76e-02 ±3.06e-03 ±1.36e-02
0.45 0.50	0.18 ±4.67e-03 ±2.74e-02	0.45 0.50	7.98e-02 ±2.76e-03 ±1.04e-02
0.50 0.55	0.16 ±4.31e-03 ±2.33e-02	0.50 0.55	6.81e-02 ±2.47e-03 ±8.44e-03
0.55 0.60	0.14 ±3.95e-03 ±2.01e-02	0.55 0.60	5.93e-02 ±2.24e-03 ±7.20e-03
0.60 0.65	0.13 ±3.56e-03 ±1.79e-02	0.60 0.65	5.15e-02 ±2.00e-03 ±6.23e-03
0.65 0.70	0.11 ±3.25e-03 ±1.56e-02	0.65 0.70	4.27e-02 ±1.77e-03 ±5.22e-03
0.70 0.75	9.84e-02 ±2.93e-03 ±1.35e-02	0.70 0.75	3.60e-02 ±1.58e-03 ±4.45e-03
0.75 0.80	8.58e-02 ±2.64e-03 ±1.18e-02	0.75 0.80	3.06e-02 ±1.41e-03 ±3.77e-03
0.80 0.90	6.76e-02 ±2.55e-03 ±9.32e-03	0.80 0.90	2.16e-02 ±1.16e-03 ±2.76e-03
0.90 1.00	4.79e-02 ±1.97e-03 ±6.67e-03	0.90 1.00	1.45e-02 ±8.79e-04 ±1.87e-03
1.00 1.10	3.61e-02 ±1.53e-03 ±4.88e-03	1.00 1.10	9.31e-03 ±6.55e-04 ±1.23e-03
1.10 1.20	2.56e-02 ±1.16e-03 ±3.44e-03	1.10 1.20	6.68e-03 ±5.00e-04 ±8.43e-04
1.20 1.30	1.87e-02 ±8.86e-04 ±2.48e-03	1.20 1.30	4.84e-03 ±4.00e-04 ±5.93e-04
1.30 1.40	1.26e-02 ±6.65e-04 ±1.70e-03	1.30 1.40	3.00e-03 ±2.88e-04 ±3.71e-04
1.40 1.50	8.64e-03 ±4.92e-04 ±1.21e-03	1.40 1.50	2.11e-03 ±2.22e-04 ±2.58e-04
1.50 1.60	6.02e-03 ±3.90e-04 ±9.02e-04	1.50 1.60	1.13e-03 ±1.66e-04 ±1.64e-04
1.60 1.70	4.25e-03 ±3.04e-04 ±7.23e-04	1.60 1.70	8.24e-04 ±1.30e-04 ±1.32e-04
1.70 1.80	3.06e-03 ±2.36e-04 ±5.03e-04		
1.80 1.90	2.07e-03 ±1.94e-04 ±3.39e-04		
1.90 2.00	1.41e-03 ±1.40e-04 ±2.22e-04		

TABLE XXVII. Invariant p_T spectra ($\frac{1}{2\pi}\frac{d^2N}{p_T dp_T dy}\pm$stat$\pm$sys (GeV/c)$^{-2}$) of primordial antiprotons in 0-10%, 10-20% and 20-40% Au+Au collisions at $\sqrt{s_{NN}}$ = 27 GeV.

p_T^{low} p_T^{high}	$\frac{1}{2\pi}\frac{d^2N}{p_T dy dp_T}$		
	0-10%	10-20%	20-40%
0.40 0.45	0.82±1.09e-02 ±0.23	0.56 ±8.25e-03 ±0.15	0.46 ±6.44e-03 ±9.58e-02
0.45 0.50	0.77±1.16e-02 ±0.18	0.56 ±8.06e-03 ±0.11	0.43 ±6.01e-03 ±7.63e-02
0.50 0.55	0.73±1.10e-02 ±0.15	0.55 ±7.82e-03 ±0.10	0.41 ±5.67e-03 ±6.64e-02
0.55 0.60	0.69±1.10e-02 ±0.13	0.52 ±7.55e-03 ±9.44e-02	0.38 ±5.35e-03 ±5.96e-02
0.60 0.65	0.65±9.90e-03 ±0.12	0.49 ±7.13e-03 ±8.42e-02	0.35 ±4.98e-03 ±5.36e-02
0.65 0.70	0.59±9.48e-03 ±0.10	0.45 ±6.64e-03 ±7.57e-02	0.32 ±4.69e-03 ±4.85e-02
0.70 0.75	0.56±8.91e-03 ±9.47e-02	0.43 ±6.21e-03 ±7.00e-02	0.29 ±4.24e-03 ±4.36e-02
0.75 0.80	0.53±8.26e-03 ±8.65e-02	0.42 ±5.78e-03 ±6.46e-02	0.26 ±3.92e-03 ±3.93e-02
0.80 0.90	0.48±9.00e-03 ±7.60e-02	0.36 ±6.85e-03 ±5.48e-02	0.22 ±4.13e-03 ±3.31e-02
0.90 1.00	0.40±7.57e-03 ±6.25e-02	0.30 ±5.63e-03 ±4.39e-02	0.17 ±3.41e-03 ±2.58e-02
1.00 1.10	0.33±6.20e-03 ±4.99e-02	0.23 ±4.48e-03 ±3.43e-02	0.13 ±2.71e-03 ±1.97e-02
1.10 1.20	0.26±4.99e-03 ±3.90e-02	0.18 ±3.55e-03 ±2.65e-02	0.10 ±2.14e-03 ±1.48e-02
1.20 1.30	0.20±3.93e-03 ±3.03e-02	0.14 ±2.75e-03 ±2.02e-02	7.50e-02 ±1.65e-03 ±1.09e-02
1.30 1.40	0.15±3.08e-03 ±2.32e-02	0.10 ±2.07e-03 ±1.53e-02	5.55e-02 ±1.27e-03 ±8.16e-03
1.40 1.50	0.12±2.39e-03 ±1.78e-02	7.70e-02 ±1.55e-03 ±1.17e-02	4.05e-02 ±9.71e-04 ±6.14e-03
1.50 1.60	8.48e-02±1.86e-03 ±1.41e-02	5.68e-02 ±1.16e-03 ±9.28e-03	3.02e-02 ±7.36e-04 ±4.87e-03
1.60 1.70	6.24e-02±1.43e-03 ±1.18e-02	4.00e-02 ±8.52e-04 ±7.63e-03	2.11e-02 ±5.60e-04 ±3.96e-03
1.70 1.80	4.45e-02±1.11e-03 ±8.28e-03	2.92e-02 ±6.28e-04 ±5.44e-03	1.50e-02 ±4.26e-04 ±2.76e-03
1.80 1.90	3.18e-02±8.61e-04 ±5.79e-03	2.01e-02 ±4.65e-04 ±3.76e-03	1.07e-02 ±3.29e-04 ±1.93e-03
1.90 2.00	2.24e-02±6.77e-04 ±4.02e-03	1.45e-02 ±3.46e-04 ±2.65e-03	7.63e-03 ±2.58e-04 ±1.34e-03

TABLE XXVIII. Invariant p_T spectra ($\frac{1}{2\pi}\frac{d^2N}{p_T dp_T dy}\pm$stat$\pm$sys (GeV/c)$^{-2}$) of primordial antiprotons in 40-60% and 60-80% Au+Au collisions at $\sqrt{s_{NN}}$ = 27 GeV.

p_T^{low} p_T^{high}	$\frac{1}{2\pi}\frac{d^2N}{p_T dy dp_T}$	p_T^{low} p_T^{high}	$\frac{1}{2\pi}\frac{d^2N}{p_T dy dp_T}$
	40-60%		60-80%
0.40 0.45	0.22 ±5.35e-03 ±5.12e-02	0.40 0.45	0.10 ±2.66e-03 ±1.89e-02
0.45 0.50	0.21 ±4.94e-03 ±4.05e-02	0.45 0.50	9.61e-02 ±2.44e-03 ±1.44e-02
0.50 0.55	0.20 ±4.47e-03 ±3.44e-02	0.50 0.55	8.54e-02 ±2.18e-03 ±1.18e-02
0.55 0.60	0.19 ±4.15e-03 ±2.97e-02	0.55 0.60	7.34e-02 ±1.94e-03 ±9.74e-03
0.60 0.65	0.17 ±3.73e-03 ±2.61e-02	0.60 0.65	6.39e-02 ±1.73e-03 ±8.28e-03
0.65 0.70	0.15 ±3.31e-03 ±2.26e-02	0.65 0.70	5.46e-02 ±1.56e-03 ±7.00e-03
0.70 0.75	0.14 ±3.02e-03 ±1.96e-02	0.70 0.75	4.62e-02 ±1.38e-03 ±5.88e-03
0.75 0.80	0.12 ±2.71e-03 ±1.71e-02	0.75 0.80	3.85e-02 ±1.19e-03 ±4.91e-03
0.80 0.90	9.88e-02 ±2.75e-03 ±1.37e-02	0.80 0.90	3.02e-02 ±1.07e-03 ±3.83e-03
0.90 1.00	7.52e-02 ±2.14e-03 ±1.02e-02	0.90 1.00	2.11e-02 ±8.26e-04 ±2.68e-03
1.00 1.10	5.43e-02 ±1.64e-03 ±7.35e-03	1.00 1.10	1.41e-02 ±6.09e-04 ±1.83e-03
1.10 1.20	3.92e-02 ±1.24e-03 ±5.31e-03	1.10 1.20	9.50e-03 ±4.54e-04 ±1.24e-03
1.20 1.30	2.80e-02 ±9.25e-04 ±3.81e-03	1.20 1.30	6.44e-03 ±3.37e-04 ±8.51e-04
1.30 1.40	2.00e-02 ±6.99e-04 ±2.75e-03	1.30 1.40	4.53e-03 ±2.57e-04 ±5.91e-04
1.40 1.50	1.44e-02 ±5.33e-04 ±2.05e-03	1.40 1.50	3.13e-03 ±2.00e-04 ±4.13e-04
1.50 1.60	9.88e-03 ±3.98e-04 ±1.54e-03	1.50 1.60	1.93e-03 ±1.44e-04 ±2.87e-04
1.60 1.70	6.88e-03 ±3.00e-04 ±1.23e-03	1.60 1.70	1.35e-03 ±1.16e-04 ±2.20e-04
1.70 1.80	4.57e-03 ±2.30e-04 ±8.23e-04	1.70 1.80	9.01e-04 ±9.50e-05 ±1.47e-04
1.80 1.90	3.23e-03 ±1.79e-04 ±5.59e-04		
1.90 2.00	2.22e-03 ±1.41e-04 ±3.78e-04		

TABLE XXIX. Invariant p_T spectra ($\frac{1}{2\pi}\frac{d^2N}{p_T dp_T dy}$±stat±sys (GeV/c)$^{-2}$) of primordial antiprotons in 0-10%, 10-20% and 20-40% Au+Au collisions at $\sqrt{s_{NN}}$ = 39 GeV.

p_T^{low}	p_T^{high}	$\frac{1}{2\pi}\frac{d^2N}{p_T dy dp_T}$		
		0-10%	10-20%	20-40%
0.40	0.45	1.11±1.08e-02 ±0.28	0.74 ±8.59e-03 ±0.18	0.56 ±5.92e-03 ±0.12
0.45	0.50	1.08±1.05e-02 ±0.23	0.73 ±8.27e-03 ±0.15	0.54 ±5.68e-03 ±9.76e-02
0.50	0.55	1.04±1.01e-02 ±0.20	0.72 ±8.07e-03 ±0.13	0.51 ±5.39e-03 ±8.55e-02
0.55	0.60	1.02±9.65e-03 ±0.18	0.70±7.68e-03 ±0.12	0.49 ±5.15e-03 ±7.78e-02
0.60	0.65	1.00±9.29e-03 ±0.16	0.67±7.35e-03 ±0.11	0.46 ±4.78e-03 ±7.11e-02
0.65	0.70	0.91±8.73e-03 ±0.15	0.63 ±6.93e-03 ±0.10	0.43 ±4.43e-03 ±6.48e-02
0.70	0.75	0.87±8.30e-03 ±0.13	0.59 ±6.52e-03 ±9.36e-02	0.39 ±4.13e-03 ±5.88e-02
0.75	0.80	0.82±7.78e-03 ±0.12	0.56 ±6.09e-03 ±8.63e-02	0.36 ±3.77e-03 ±5.32e-02
0.80	0.90	0.73±8.89e-03 ±0.11	0.50 ±7.44e-03 ±7.46e-02	0.31 ±4.26e-03 ±4.46e-02
0.90	1.00	0.61±7.47e-03 ±8.85e-02	0.41 ±6.15e-03 ±6.00e-02	0.24 ±3.53e-03 ±3.50e-02
1.00	1.10	0.50±6.19e-03 ±7.10e-02	0.33 ±4.91e-03 ±4.74e-02	0.19 ±2.80e-03 ±2.71e-02
1.10	1.20	0.40±4.97e-03 ±5.64e-02	0.26 ±3.88e-03 ±3.69e-02	0.15 ±2.18e-03 ±2.05e-02
1.20	1.30	0.31±3.93e-03 ±4.38e-02	0.20 ±3.00e-03 ±2.84e-02	0.11 ±1.70e-03 ±1.54e-02
1.30	1.40	0.23±3.06e-03 ±3.36e-02	0.15 ±2.28e-03 ±2.16e-02	8.06e-02 ±1.28e-03 ±1.15e-02
1.40	1.50	0.17±2.34e-03 ±2.59e-02	0.11 ±1.71e-03 ±1.66e-02	5.75e-02 ±9.68e-04 ±8.67e-03
1.50	1.60	0.12±1.78e-03 ±2.05e-02	8.09e-02 ±1.26e-03 ±1.31e-02	4.04e-02 ±7.22e-04 ±6.72e-03
1.60	1.70	8.98e-02±1.35e-03 ±1.71e-02	5.90e-02 ±9.39e-04 ±1.10e-02	2.86e-02 ±5.33e-04 ±5.55e-03
1.70	1.80	6.41e-02±1.02e-03 ±1.21e-02	4.26e-02 ±6.75e-04 ±7.86e-03	2.00e-02 ±4.00e-04 ±3.87e-03
1.80	1.90	4.62e-02±7.67e-04 ±8.57e-03	3.02e-02 ±4.88e-04 ±5.54e-03	1.30e-02 ±2.93e-04 ±2.66e-03
1.90	2.00	3.24e-02±5.82e-04 ±5.96e-03	2.14e-02 ±3.54e-04 ±3.87e-03	9.50e-03 ±2.19e-04 ±1.83e-03

TABLE XXX. Invariant p_T spectra ($\frac{1}{2\pi}\frac{d^2N}{p_T dp_T dy}$±stat±sys (GeV/c)$^{-2}$) of primordial antiprotons in 40-60% and 60-80% Au+Au collisions at $\sqrt{s_{NN}}$ = 39 GeV.

p_T^{low}	p_T^{high}	$\frac{1}{2\pi}\frac{d^2N}{p_T dy dp_T}$	p_T^{low}	p_T^{high}	$\frac{1}{2\pi}\frac{d^2N}{p_T dy dp_T}$
		40-60%			60-80%
0.40	0.45	0.30 ±5.01e-03 ±7.16e-02	0.40	0.45	0.14 ±2.33e-03 ±2.47e-02
0.45	0.50	0.28 ±4.52e-03 ±5.58e-02	0.45	0.50	0.13 ±2.17e-03 ±1.85e-02
0.50	0.55	0.27 ±4.26e-03 ±4.68e-02	0.50	0.55	0.12 ±1.92e-03 ±1.50e-02
0.55	0.60	0.25 ±3.85e-03 ±4.00e-02	0.55	0.60	0.10 ±1.74e-03 ±1.27e-02
0.60	0.65	0.23 ±3.49e-03 ±3.45e-02	0.60	0.65	8.97e-02 ±1.56e-03 ±1.10e-02
0.65	0.70	0.20 ±3.07e-03 ±2.99e-02	0.65	0.70	7.69e-02 ±1.40e-03 ±9.40e-03
0.70	0.75	0.18 ±2.83e-03 ±2.60e-02	0.70	0.75	6.69e-02 ±1.23e-03 ±8.20e-03
0.75	0.80	0.16 ±2.52e-03 ±2.27e-02	0.75	0.80	5.78e-02 ±1.11e-03 ±7.13e-03
0.80	0.90	0.13 ±2.74e-03 ±1.82e-02	0.80	0.90	4.34e-02 ±1.09e-03 ±5.50e-03
0.90	1.00	0.10 ±2.11e-03 ±1.37e-02	0.90	1.00	3.05e-02 ±8.17e-04 ±3.95e-03
1.00	1.10	7.57e-02 ±1.63e-03 ±1.01e-02	1.00	1.10	2.14e-02 ±6.20e-04 ±2.78e-03
1.10	1.20	5.62e-02 ±1.25e-03 ±7.46e-03	1.10	1.20	1.49e-02 ±4.81e-04 ±1.92e-03
1.20	1.30	4.14e-02 ±9.30e-04 ±5.52e-03	1.20	1.30	1.03e-02 ±3.42e-04 ±1.33e-03
1.30	1.40	2.95e-02 ±7.00e-04 ±4.02e-03	1.30	1.40	6.90e-03 ±2.50e-04 ±9.07e-04
1.40	1.50	2.08e-02 ±5.22e-04 ±2.96e-03	1.40	1.50	4.72e-03 ±1.93e-04 ±6.39e-04
1.50	1.60	1.45e-02 ±3.85e-04 ±2.26e-03	1.50	1.60	3.09e-03 ±1.35e-04 ±4.60e-04
1.60	1.70	1.03e-02 ±2.79e-04 ±1.85e-03	1.60	1.70	2.15e-03 ±1.02e-04 ±3.72e-04
1.70	1.80	7.21e-03 ±2.06e-04 ±1.27e-03	1.70	1.80	1.50e-03 ±7.60e-05 ±2.49e-04
1.80	1.90	5.23e-03 ±1.60e-04 ±9.02e-04	1.80	1.90	9.77e-04 ±5.20e-05 ±1.63e-04
1.90	2.00	3.52e-03 ±1.28e-04 ±6.04e-04	1.90	2.00	6.27e-04 ±4.50e-05 ±1.07e-04

TABLE XXXI. Invariant p_T spectra ($\frac{1}{2\pi}\frac{d^2N}{p_T dp_T dy}\pm$stat$\pm$sys (GeV/c)$^{-2}$) of primordial antiprotons in 0-10%, 10-20% and 20-40% Au+Au collisions at $\sqrt{s_{NN}}$ = 62.4 GeV.

p_T^{low} p_T^{high}	$\frac{1}{2\pi}\frac{d^2N}{p_T dy dp_T}$		
	0-10%	10-20%	20-40%
0.50 0.60	0.86 ±0.13 ±0.23	0.78 ±0.11 ±0.18	0.50 ±5.58e-02 ±0.10
0.60 0.70	0.99 ±0.10 ±0.21	0.69 ±8.89e-02 ±0.19	0.51 ±4.96e-02 ±9.12e-02
0.70 0.80	0.99 ±9.11e-02 ±0.19	0.72 ±7.57e-02 ±0.17	0.43 ±3.86e-02 ±7.92e-02
0.80 0.90	0.83 ±7.30e-02 ±0.16	0.55 ±5.96e-02 ±0.14	0.35 ±3.24e-02 ±6.71e-02
0.90 1.00	0.84 ±6.73e-02 ±0.14	0.56 ±5.21e-02 ±0.11	0.32 ±2.82e-02 ±5.51e-02
1.00 1.20	0.76 ±4.10e-02 ±0.11	0.52 ±3.37e-02 ±6.58e-02	0.31 ±1.81e-02 ±4.38e-02
1.20 1.40	0.42 ±2.50e-02 ±6.14e-02	0.30 ±2.04e-02 ±3.37e-02	0.14 ±1.02e-02 ±2.28e-02
1.40 1.60	0.23 ±1.57e-02 ±3.39e-02	0.13 ±1.23e-02 ±1.82e-02	7.40e-02 ±6.35e-03 ±1.20e-02
1.60 1.80	0.12 ±1.01e-02 ±1.79e-02	7.63e-02 ±8.05e-03 ±9.26e-03	4.00e-02 ±3.96e-03 ±6.32e-03
1.80 2.00	6.26e-02 ±6.82e-03 ±9.21e-03	3.65e-02 ±5.28e-03 ±8.33e-03	2.40e-02 ±2.74e-03 ±3.43e-03
2.00 2.50	2.43e-02 ±2.45e-03 ±3.62e-03	2.81e-02 ±1.93e-03 ±3.07e-03	9.00e-03 ±9.52e-04 ±1.15e-03
2.50 3.00	3.88e-03 ±4.68e-04 ±8.23e-04	2.62e-03 ±3.49e-04 ±5.67e-04	2.00e-03 ±7.50e-05 ±3.46e-04

TABLE XXXII. Invariant p_T spectra ($\frac{1}{2\pi}\frac{d^2N}{p_T dp_T dy}\pm$stat$\pm$sys (GeV/c)$^{-2}$) of primordial antiprotons in 40-80% Au+Au collisions at $\sqrt{s_{NN}}$ = 62.4 GeV.

p_T^{low} p_T^{high}	$\frac{1}{2\pi}\frac{d^2N}{p_T dy dp_T}$
	40-80%
0.50 0.60	0.20 ±2.51e-02 ±3.29e-02
0.60 0.70	0.14 ±1.78e-02 ±2.60e-02
0.70 0.80	0.12 ±1.49e-02 ±2.15e-02
0.80 0.90	8.72e-02 ±1.12e-02 ±1.66e-02
0.90 1.00	8.65e-02 ±1.01e-02 ±1.42e-02
1.00 1.20	6.29e-02 ±5.73e-03 ±9.72e-03
1.20 1.40	2.68e-02 ±3.25e-03 ±4.74e-03
1.40 1.60	1.33e-02 ±1.92e-03 ±2.43e-03
1.60 1.80	6.66e-03 ±1.21e-03 ±1.21e-03
1.80 2.00	3.16e-03 ±7.18e-04 ±5.61e-04
2.00 2.50	1.68e-03 ±3.09e-04 ±2.08e-04
2.50 3.00	3.54e-04 ±3.90e-05 ±6.40e-05

Appendix C: Integral dN/dy of primordial (anti)protons and feed-down fractions

TABLE XXXIII. Summary of extracted yield dN/dy of the primordial protons for Au+Au collisions at each collision energy (GeV). The first error on dN/dy is the statistical uncertainty and the second one is the systematic uncertainty.

Collision energy (GeV)	dN/dy		
	0-10%	10-20%	20-40%
7.7	38.26±0.11±5.61	25.37±0.05±3.88	15.38±0.05±2.66
11.5	28.82±0.07±4.83	18.70±0.04±3.30	10.60±0.03±2.10
14.5	26.03±0.07±4.41	17.48±0.05±2.92	9.55±0.04±1.66
19.6	20.96±0.06±4.20	14.80±0.04±3.00	7.99±0.03±1.83
27	19.28±0.04±3.56	12.63±0.03±2.47	7.17±0.02±1.59
39	15.53±0.03±2.78	10.56±0.03±2.05	6.20±0.02±1.35
54.4	14.38±0.11±1.42	9.45 ±0.09±0.94	5.28±0.05±0.56
62.4	16.11±0.24±1.63	11.10±0.20±1.05	5.91±0.05±0.82
200	15.85±0.98±1.99	12.43±0.84±1.47	7.40±0.46±0.76

TABLE XXXIV. Summary of extracted yield dN/dy of the primordial protons for Au+Au collisions at each collision energy (GeV). The first error on dN/dy is the statistical uncertainty and the second one is the systematic uncertainty.

Collision energy (GeV)	dN/dy	
	40-60%	60-80%
7.7	5.95±0.04±1.44	1.77±0.02±0.65
11.5	4.18±0.02±1.16	1.14±0.01±0.53
14.5	3.54±0.02±0.61	0.93±0.01±0.16
19.6	3.20±0.02±0.95	0.97±0.01±0.42
27	3.05±0.01±0.88	$(9.08±0.06±4.36)×10^{-1}$
39	2.53±0.01±0.77	$(7.98±0.04±3.57)×10^{-1}$
54.4	2.10±0.03±0.22	$(6.28±0.15±0.60)×10^{-1}$
62.4	1.52±0.03±0.15	
200	3.46±0.21±0.32	1.15±0.08±0.12

TABLE XXXV. Summary of extracted yield dN/dy of the primordial antiprotons for Au+Au collisions at each collision energy (GeV). The first error on dN/dy is the statistical uncertainty and the second one is the systematic uncertainty.

Collision energy (GeV)	dN/dy		
	0-10%	10-20%	20-40%
7.7	$(1.60±0.15±0.48)×10^{-1}$	$(1.22±0.06±0.36)×10^{-1}$	$(7.69±0.62±2.53)×10^{-2}$
11.5	$(6.64±0.22±1.79)×10^{-1}$	$(4.61±0.11±1.28)×10^{-1}$	$(2.88±0.10±0.91)×10^{-1}$
14.5	1.33±0.02±0.26	$(9.56±0.11±2.16)×10^{-1}$	$(6.53±0.15±1.05)×10^{-1}$
19.6	2.05±0.02±0.51	1.44±0.01±0.38	$(9.38±0.10±2.64)×10^{-1}$
27	3.02±0.02±0.70	2.13±0.01±0.52	1.35±0.01±0.36
39	4.51±0.01±0.98	2.90±0.01±0.70	1.88±0.01±0.49
62.4	5.24±0.13±1.11	3.82±0.11±0.79	2.53±0.03±0.31

TABLE XXXVI. Summary of extracted yield dN/dy of the primordial antiprotons for Au+Au collisions at each collision energy (GeV). The first error on dN/dy is the statistical uncertainty and the second one is the systematic uncertainty.

Collision energy (GeV)	dN/dy	
	40-60%	60-80%
7.7	$(3.98\pm0.48\pm1.60)\times10^{-2}$	$(1.58\pm0.25\pm0.80)\times10^{-2}$
11.5	$(1.04\pm0.04\pm0.59)\times10^{-1}$	$(4.56\pm0.37\pm3.25)\times10^{-2}$
14.5	$(2.87\pm0.06\pm0.56)\times10^{-1}$	$(8.71\pm0.36\pm1.52)\times10^{-2}$
19.6	$(4.71\pm0.05\pm1.64)\times10^{-1}$	$(1.84\pm0.04\pm0.86)\times10^{-1}$
27	$(6.18\pm0.06\pm2.25)\times10^{-1}$	$(2.30\pm0.03\pm1.27)\times10^{-1}$
39	$(8.76\pm0.04\pm3.06)\times10^{-1}$	$(3.23\pm0.02\pm1.59)\times10^{-1}$
62.4	$(6.49\pm0.23\pm7.86)\times10^{-1}$	

TABLE XXXVII. Summary of extracted feed-down fractions based on the data driven method for Au+Au collisions at each collision energy (GeV). The first error on fraction is the statistical uncertainty and the second one is the systematic uncertainty.

Collision energy (GeV)	Proton feed-down fraction (%)		
	0-10%	10-20%	20-40%
7.7	23.76±0.12±2.97	24.00±0.13±3.05	21.15±0.12±3.08
11.5	27.19±0.09±3.62	28.32±0.11±3.85	28.33±0.12±4.26
14.5	27.18±0.17±3.88	28.03±0.20±3.63	28.04±0.20±3.75
19.6	32.68±0.17±4.63	31.63±0.20±4.58	33.10±0.21±5.37
27	33.07±0.15±4.33	34.15±0.18±4.63	34.18±0.17±5.23
39	36.19±0.13±4.42	37.72±0.16±4.92	36.16±0.15±5.22
54.4	39.08±0.26±2.98	39.68±0.33±3.01	40.34±0.33±3.47
62.4	41.20±0.00±4.25	38.99±0.00±3.88	38.42±0.00±3.09
200	44.00±2.58±5.48	37.15±2.40±4.37	37.08±2.18±4.63

TABLE XXXVIII. Summary of extracted feed-down fractions based on the data driven method for Au+Au collisions at each collision energy (GeV). The first error on fraction is the statistical uncertainty and the second one is the systematic uncertainty.

Collision energy (GeV)	Proton feed-down fraction (%)	
	40-60%	60-80%
7.7	19.07±0.19±3.86	15.14±0.23±4.77
11.5	27.07±0.19±5.63	27.04±0.28±9.19
14.5	27.22±0.33±3.95	24.85±0.44±4.30
19.6	29.65±0.32±6.40	25.13±0.39±8.28
27	30.49±0.27±6.31	27.21±0.34±9.76
39	32.95±0.23±6.72	29.68±0.31±9.72
54.4	38.94±0.57±3.25	35.81±0.89±3.15
62.4	31.44±2.34	
200	30.31±1.77±4.03	32.57±2.29±1.62

TABLE XXXIX. Summary of extracted feed-down fractions based on the data driven method for Au+Au collisions at each collision energy (GeV). The first error on fraction is the statistical uncertainty and the second one is the systematic uncertainty.

Collision energy (GeV)	Antiproton feed-down fraction (%)		
	0-10%	10-20%	20-40%
7.7	55.43±2.26±7.99	52.93±1.19±8.06	53.19±2.02±8.57
11.5	49.51±0.85±7.42	51.43±0.64±7.39	51.47±0.85±8.24
14.5	42.53±0.46±6.27	42.14±0.36±7.44	39.12±0.59±4.84
19.6	45.62±0.32±6.62	47.12±0.30±6.88	44.99±0.32±7.26
27	45.53±0.24±6.31	47.09±0.23±6.51	44.88±0.25±6.88
39	43.10±0.13±5.82	46.45±0.16±6.34	44.42±0.15±6.76
62.4	45.89±4.50	47.01±3.78	47.00±3.97

TABLE XL. Summary of extracted feed-down fractions based on the data driven method for Au+Au collisions at each collision energy (GeV). The first error on fraction is the statistical uncertainty and the second one is the systematic uncertainty.

Collision energy (GeV)	Antiproton feed-down fraction (%)	
	40-60%	60-80%
7.7	48.36±3.03±10.45	37.13±3.64±12.74
11.5	61.82±1.03±13.60	52.04±2.05±18.04
14.5	39.12±0.62±5.07	36.51±1.11±4.47
19.6	39.20±0.38±8.51	30.81±0.55±10.17
27	44.53±0.35±9.27	35.94±0.42±12.89
39	41.67±0.24±8.76	33.73±0.31±11.11
62.4	49.19±3.94	

Appendix D: Fraction of the measured and extrapolated yield for primordial proton, deuteron, and triton

TABLE XLI. Fraction of the measured and extrapolated yield for primordial proton at 0-10% centrality in Au+Au collisions at $\sqrt{s_{NN}}$ = 7.7 - 200 GeV. For the extrapolation, a Blast-Wave fit is used in all cases.

Collision energy (GeV)	Proton 0-10%		
	Measured dN/dy	Extrapolated dN/dy	
		Low p_T	High p_T
Measured range p_T = 0.4 - 2.0 GeV/c			
7.7	80.32%	18.09%	1.59%
11.5	80.09%	18.42%	1.49%
Measured range p_T = 0.5 - 2.0 GeV/c			
14.5	72.54%	25.57%	1.89%
Measured range p_T = 0.4 - 2.0 GeV/c			
19.6	80.94%	17.03%	2.03%
27	81.18%	16.57%	2.25%
39	81.50%	15.67%	2.83%
Measured range p_T = 0.4 - 2.2 GeV/c			
54.4	82.67%	15.80%	1.53%
Measured range p_T = 0.5 - 3.0 GeV/c			
62.4	80.14%	19.74%	0.12%
Measured range p_T = 0.5 - 12.0 GeV/c			
200	86.18%	13.82%	0

TABLE XLII. Fraction of the measured and extrapolated yield for primordial proton at 10-20% centrality in Au+Au collisions at $\sqrt{s_{NN}}$ = 7.7 - 200 GeV. For the extrapolation, a Blast-Wave fit is used in all cases.

Collision energy (GeV)	Proton 10-20%		
	Measured dN/dy	Extrapolated dN/dy	
		Low p_T	High p_T
Measured range p_T = 0.4 - 2.0 GeV/c			
7.7	79.09%	19.82%	1.09%
11.5	79.92%	18.70%	1.38%
Measured range p_T = 0.5 - 2.0 GeV/c			
14.5	71.94%	26.42%	1.64%
Measured range p_T = 0.4 - 2.0 GeV/c			
19.6	80.73%	17.40%	1.87%
27	80.90%	17.12%	1.98%
39	81.26%	16.30%	2.44%
Measured range p_T = 0.4 - 2.2 GeV/c			
54.4	82.54%	16.08%	1.38%
Measured range p_T = 0.5 - 3.0 GeV/c			
62.4	81.13%	18.68%	0.19%
Measured range p_T = 0.5 - 10.0 GeV/c			
200	86.05%	13.95%	0

TABLE XLIII. Fraction of the measured and extrapolated yield for primordial proton 20-40% centrality in Au+Au collisions at $\sqrt{s_{NN}}$ = 7.7 - 200 GeV. For the extrapolation, a Blast-Wave fit is used in all cases.

Collision energy (GeV)	Proton 20-40%		
	Measured dN/dy	Extrapolated dN/dy	
		Low p_T	High p_T
Measured range p_T = 0.4 - 2.0 GeV/c			
7.7	78.48%	20.64%	0.88%
11.5	79.33%	19.57%	1.10%
Measured range p_T = 0.5 - 2.0 GeV/c			
14.5	71.02%	27.62%	1.36%
Measured range p_T = 0.4 - 2.0 GeV/c			
19.6	79.24%	19.64%	1.12%
27	80.27%	18.22%	1.51%
39	80.78%	17.32%	1.90%
Measured range p_T = 0.4 - 2.2 GeV/c			
54.4	82.07%	16.78%	1.15%
Measured range p_T = 0.5 - 3.0 GeV/c			
62.4	78.62%	21.18%	0.20%
Measured range p_T = 0.5 - 10.0 GeV/c			
200	83.03%	16.97%	0

TABLE XLIV. Fraction of the measured and extrapolated yield for primordial proton at 40-60% centrality in Au+Au collisions at $\sqrt{s_{NN}}$ = 7.7 - 200 GeV. For the extrapolation, a Blast-Wave fit is used in all cases.

Collision energy (GeV)	Proton 40-60%		
	Measured dN/dy	Extrapolated dN/dy	
		Low p_T	High p_T
Measured range p_T = 0.4 - 2.0 GeV/c			
7.7	73.76%	25.73%	0.51%
11.5	72.87%	26.47%	0.66%
Measured range p_T = 0.5 - 2.0 GeV/c			
14.5	70.20%	28.67%	1.13%
Measured range p_T = 0.4 - 2.0 GeV/c			
19.6	74.49%	24.52%	0.99%
27	78.68%	20.44%	0.88%
39	77.04%	21.25%	1.71%
Measured range p_T = 0.4 - 2.2 GeV/c			
54.4	82.56%	16.57%	0.87%
Measured range p_T = 0.5 - 3.0 GeV/c			
62.4(40-80%)	74.29%	25.61%	0.10%
Measured range p_T = 0.5 - 10.0 GeV/c			
200	79.39%	20.61%	0

TABLE XLV. Fraction of the measured and extrapolated yield for primordial proton at 60-80% centrality in Au+Au collisions at $\sqrt{s_{NN}}$ = 7.7 - 200 GeV. For the extrapolation, a Blast-Wave fit is used in all cases.

Collision energy (GeV)	Proton 60-80%		
	Measured dN/dy	Extrapolated dN/dy	
		Low p_T	High p_T
Measured range p_T = 0.4 - 2.0 GeV/c			
7.7	68.31%	31.48%	0.21%
11.5	70.12%	29.57%	0.31%
Measured range p_T = 0.5 - 2.0 GeV/c			
14.5	66.60%	33.03%	0.37%
Measured range p_T = 0.4 - 2.0 GeV/c			
19.6	71.69%	27.82%	0.49%
27	72.63%	26.81%	0.56%
39	72.84%	26.50%	0.66%
Measured range p_T = 0.4 - 2.2 GeV/c			
54.4	75.74%	23.75%	0.51%
Measured range p_T = 0.5 - 3.0 GeV/c			
62.4(40-80%)	74.29%	25.61%	0.10%
Measured range p_T = 0.5 - 8.0 GeV/c			
200	71.72%	28.28%	0

TABLE XLVI. Fraction of the measured and extrapolated yield for deuteron at 0-10% centrality in Au+Au collisions at $\sqrt{s_{NN}}$ = 7.7 - 200 GeV. For the extrapolation, a Blast-Wave fit is used in all cases.

Collision energy (GeV)	Deuteron 0-10%		
	Measured dN/dy	Extrapolated dN/dy	
		Low p_T	High p_T
Measured range p_T = 0.6 - 4.8 GeV/c			
7.7	84.53%	15.46%	2.52e-3%
11.5	84.61%	15.38%	5.47e-3%
14.5	84.49%	15.50%	5.72e-3%
19.6	85.91%	14.08%	5.42e-3%
27	86.11%	13.88%	0.01%
39	87.44%	12.55%	7.85e-3%
Measured range p_T = 0.6 - 5.0 GeV/c			
54.4	87.04%	12.95%	6.46e-3%
Measured range p_T = 0.6 - 4.8 GeV/c			
62.4	87.87%	12.11%	0.02%
Measured range p_T = 1.0 - 4.8 GeV/c			
200	73.78%	26.16%	0.06%

TABLE XLVII. Fraction of the measured and extrapolated yield for deuteron at 10-20% centrality in Au+Au collisions at $\sqrt{s_{NN}}$ = 7.7 - 200 GeV. For the extrapolation, a Blast-Wave fit is used in all cases.

Collision energy (GeV)	Deuteron 10-20%		
	Measured dN/dy	Extrapolated dN/dy	
		Low p_T	High p_T
Measured range p_T = 0.6 - 4.8 GeV/c			
7.7	83.56%	16.43%	1.80e-3%
11.5	83.89%	16.10%	3.34e-3%
14.5	83.48%	16.51%	4.83e-3%
19.6	84.46%	15.53%	4.45e-3%
27	84.93%	15.06%	9.47e-3%
39	86.32%	13.67%	9.50e-3%
Measured range p_T = 0.6 - 5.0 GeV/c			
54.4	87.06%	12.93%	6.13e-3%
Measured range p_T = 0.6 - 4.8 GeV/c			
62.4	86.93%	13.05%	0.02%
Measured range p_T = 0.8 - 4.8 GeV/c			
200	81.41%	18.53%	0.06%

TABLE XLVIII. Fraction of the measured and extrapolated yield for deuteron at 20-40% centrality in Au+Au collisions at $\sqrt{s_{NN}}$ = 7.7 - 200 GeV. For the extrapolation, a Blast-Wave fit is used in all cases.

Collision energy (GeV)	Deuteron 20-40%		
	Measured dN/dy	Extrapolated dN/dy	
		Low p_T	High p_T
Measured range p_T = 0.6 - 4.8 GeV/c			
7.7	80.24%	19.75%	1.19e-3%
11.5	80.57%	19.42%	2.82e-3%
14.5	81.18%	18.81%	2.95e-3%
19.6	81.80%	18.19%	4.24e-3%
27	82.50%	17.49%	7.14e-3%
39	83.75%	16.24%	8.68e-3%
Measured range p_T = 0.6 - 5.0 GeV/c			
54.4	84.70%	15.29%	4.12e-3%
Measured range p_T = 0.6 - 4.8 GeV/c			
62.4	84.34%	15.65%	9.48e-3%
200	87.59%	12.37%	0.04%

TABLE XLIX. Fraction of the measured and extrapolated yield for deuteron at different 40-60% centrality in Au+Au collisions at $\sqrt{s_{NN}}$ = 7.7 - 200 GeV. For the extrapolation, a Blast-Wave fit is used in all cases.

Collision energy (GeV)	Deuteron 40-60%		
	Measured dN/dy	Extrapolated dN/dy	
		Low p_T	High p_T
Measured range p_T = 0.6 - 4.0 GeV/c			
7.7	73.24%	26.75%	8.55e-3%
11.5	74.81%	25.18%	0.01%
14.5	74.83%	25.15%	0.02%
19.6	75.54%	24.44%	0.02%
27	76.87%	23.10%	0.03%
Measured range p_T = 0.6 - 4.8 GeV/c			
39	78.12%	21.87%	3.23e-3%
Measured range p_T = 0.6 - 4.6 GeV/c			
54.4	79.0%	20.99%	7.30e-3%
Measured range p_T = 0.6 - 4.8 GeV/c			
62.4	79.93%	20.06%	3.75e-3%
Measured range p_T = 1.0 - 4.8 GeV/c			
200	56.57%	43.40%	0.03%

TABLE L. Fraction of the measured and extrapolated yield for deuteron at 60-80% centrality in Au+Au collisions at $\sqrt{s_{NN}}$ = 7.7 - 200 GeV. For the extrapolation, a Blast-Wave fit is used in all cases.

Collision energy (GeV)	Deuteron 60-80%		
	Measured dN/dy	Extrapolated dN/dy	
		Low p_T	High p_T
Measured range p_T = 0.6 - 2.8 GeV/c			
7.7	65.22%	34.70%	0.08%
Measured range p_T = 0.6 - 3.2 GeV/c			
11.5	67.97%	31.99%	0.04%
14.5	67.94%	32.02%	0.04%
19.6	69.31%	30.64%	0.05%
Measured range p_T = 0.6 - 4.0 GeV/c			
27	70.04%	29.95%	3.18e-3%
39	72.16%	27.83%	5.82e-3%
Measured range p_T = 0.6 - 3.8 GeV/c			
54.4	73.01%	26.97%	0.02%
Measured range p_T = 0.6 - 4.0 GeV/c			
62.4	73.35%	26.64%	8.15e-3%
Measured range p_T = 1.0 - 4.0 GeV/c			
200	47.19%	52.77%	0.04%

TABLE LI. Fraction of the measured and extrapolated yield for triton at 0-10% centrality in Au+Au collisions at $\sqrt{s_{NN}}$ = 7.7 - 200 GeV. For the extrapolation, a Blast-Wave fit is used in all cases.

Collision energy (GeV)	Triton 0-10%		
	Measured dN/dy	Extrapolated dN/dy	
		Low p_T	High p_T
Measured range p_T = 1.2 - 4.2 GeV/c			
7.7	68.27%	31.58%	0.15%
11.5	68.84%	30.75%	0.41%
14.5	69.41%	30.32%	0.27%
19.6	68.84%	30.66%	0.50%
27	69.93%	29.28%	0.79%
39	72.22%	27.33%	0.45%
54.4	73.80%	25.60%	0.60%
Measured range p_T = 1.2 - 3.0 GeV/c			
62.4	64.84%	26.50%	8.66%
Measured range p_T = 1.5 - 3.0 GeV/c			
200	52.75%	34.22%	13.03%

TABLE LII. Fraction of the measured and extrapolated yield for triton at 10-20% centrality in Au+Au collisions at $\sqrt{s_{NN}}$ = 7.7 - 200 GeV. For the extrapolation, a Blast-Wave fit is used in all cases.

Collision energy (GeV)	Triton 10-20%		
	Measured dN/dy	Extrapolated dN/dy	
		Low p_T	High p_T
Measured range p_T = 1.2 - 4.2 GeV/c			
7.7	63.31%	36.58%	0.11%
11.5	65.64%	34.13%	0.23%
14.5	63.53%	36.22%	0.25%
19.6	67.35%	32.30%	0.35%
27	68.29%	31.31%	0.40%
39	70.03%	29.66%	0.31%
54.4	71.15%	28.42%	0.43%
Measured range p_T = 1.2 - 3.0 GeV/c			
62.4	63.80%	30.85%	5.35%
Measured range p_T = 1.5 - 3.0 GeV/c			
200	53.82%	38.55%	7.63%

TABLE LIII. Fraction of the measured and extrapolated yield for triton at 20-40% centrality in Au+Au collisions at $\sqrt{s_{NN}}$ = 7.7 - 200 GeV. For the extrapolation, a Blast-Wave fit is used in all cases.

Collision energy (GeV)	Triton 20-40%		
	Measured dN/dy	Extrapolated dN/dy	
		Low p_T	High p_T
Measured range p_T = 1.2 - 4.2 GeV/c			
7.7	56.93%	42.93%	0.14%
11.5	57.91%	41.99%	0.10%
14.5	58.51%	41.37%	0.12%
19.6	61.26%	38.61%	0.13%
27	64.48%	35.23%	0.29%
39	63.56%	36.14%	0.30%
54.4	65.40%	34.31%	0.29%
Measured range p_T = 1.2 - 3.0 GeV/c			
62.4	63.89%	30.81%	5.30%
Measured range p_T = 1.5 - 3.0 GeV/c			
200	51.26%	40.44%	8.30%

TABLE LIV. Fraction of the measured and extrapolated yield for triton at 40-80% centrality in Au+Au collisions at $\sqrt{s_{\mathrm{NN}}}$ = 7.7 - 200 GeV. For the extrapolation, a Blast-Wave fit is used in all cases.

Collision energy (GeV)	Triton 40-80%		
	Measured dN/dy	Extrapolated dN/dy	
		Low p_T	High p_T
Measured range p_T = 1.2 - 3.6 GeV/c			
7.7	40.50%	58.90%	0.60%
11.5	43.99%	55.76%	0.25%
14.5	44.56%	55.19%	0.25%
19.6	46.91%	52.66%	0.43%
27	49.46%	50.28%	0.26%
39	48.38%	51.20%	0.42%
54.4	48.92%	50.57%	0.51%
Measured range p_T = 1.2 - 3.0 GeV/c			
62.4	57.44%	39.87%	2.69%
Measured range p_T = 1.5 - 3.0 GeV/c			
200	47.01%	50.21%	2.78%

[1] M. Tanabashi *et al.* [Particle Data Group], Phys. Rev. D **98**, no.3, 030001 (2018)

[2] W. Zhao, K. j. Sun, C. M. Ko and X. Luo, Phys. Lett. B **820**, 136571 (2021)

[3] L. Adamczyk *et al.* [STAR], Phys. Rev. C **96**, no.4, 044904 (2017)

[4] B. I. Abelev *et al.* [STAR], Phys. Rev. C **79**, 034909 (2009)

[5] J. Adam *et al.* [STAR], Phys. Rev. C **101**, no.2, 024905 (2020)

[6] B. I. Abelev *et al.* [STAR], Phys. Lett. B **655**, 104-113 (2007)

[7] B. I. Abelev *et al.* [STAR], Phys. Rev. Lett. **97**, 152301 (2006)

[8] M. M. Aggarwal *et al.* [STAR], Phys. Rev. C **83**, 024901 (2011)

[9] J. Adam *et al.* [STAR], Phys. Rev. C **102**, no.3, 034909 (2020)

[10] L. Adamczyk *et al.* [STAR], Phys. Rev. Lett. **121**, no.3, 032301 (2018)

[11] J. Adam *et al.* [ALICE], Eur. Phys. J. C **75**, no.5, 226 (2015)

[12] S. Acharya *et al.* [ALICE], Phys. Lett. B **794**, 50-63 (2019)

[13] S. Acharya *et al.* [ALICE], Phys. Rev. C **97**, no.2, 024615 (2018)

[14] S. Acharya *et al.* [ALICE], Phys. Lett. B **800**, 135043 (2020)

[15] S. Acharya *et al.* [ALICE], Phys. Rev. C **101**, no.4, 044906 (2020)

[16] B. Abelev *et al.* [ALICE], Phys. Rev. C **88**, 044910 (2013)

[17] J. Adam *et al.* [ALICE], Phys. Rev. C **93**, no.2, 024917 (2016)

[18] K. J. Sun, C. M. Ko and B. Dönigus, Phys. Lett. B **792**, 132-137 (2019)

[19] V. Vovchenko, B. Dönigus and H. Stoecker, Phys. Lett. B **785**, 171-174 (2018)